An evolutionary trade-off between parasite virulence and dispersal at experimental invasion fronts

Louise Solveig Nørgaard, Giacomo Zilio, Camille Saade, Claire Gougat-barbera, Matthew D Hall, Emanuel A Fronhofer, Oliver Kaltz

An evolutionary trade-off between parasite virulence and dispersal at experimental invasion fronts

Louise Solveig Nørgaard[1,2#*], Giacomo Zilio[2#], Camille Saade[2],

Claire Gougat-Barbera[2], Matthew D. Hall[1], Emanuel A. Fronhofer[2] & Oliver Kaltz[2*]

[1]School of Biological Sciences and Centre for Geometric Biology, Monash University, Melbourne 3800, Australia

[2]ISEM, University of Montpellier, CNRS, EPHE, IRD, Montpellier, France.

*Corresponding author: oliver.kaltz@umontpellier.fr; lnorga10@hotmail.com

#Shared first author contribution

1

12
13 **ABSTRACT**

14   Eco-evolutionary processes may play an important role in the spatial spread of infectious disease.

15   Current theory predicts more exploitative parasites to evolve in highly connected populations or at the

16   front of spreading epidemics. However, many parasites rely on host dispersal to reach new populations.

17   This may lead to conflict between local transmission and global spread, possibly counteracting selection

18   for higher virulence. Here, we used the freshwater host *Paramecium caudatum* and its bacterial parasite

19   *Holospora undulata* to investigate parasite evolution under an experimental range expansion scenario

20   with natural host dispersal. We find that parasites evolving at experimental range fronts favoured higher

21   dispersal rates of infected hosts than did parasites evolving in core populations. Front parasites further

22   showed lower levels of virulence (host division and survival) and delayed development of infection,

23   consistent with parameter estimates from an epidemiological model that we fitted on experimental time-

24   series data. This combined evidence suggests an evolutionary trade-off between virulence and host-

25   mediated dispersal, with a concomitant reduction in the investment into horizontal transmission. Our

26   experiment illustrates how parasite evolution can be shaped by divergent selection encountered in

27   different segments of an epidemic wave. Such an interplay between demography and spatial selection

28   has important implications for the understanding and management of emerging diseases, and, more

29   generally, for biological invasions and other non-equilibrium scenarios of spreading populations.

30

34
35

36 **SIGNIFICANCE STATEMENT**

37 What drives parasite evolution in spatially expanding epidemics? Many parasites require dispersal of

38 infected hosts to reach new patches, and this may produce specific adaptations enhancing spatial spread.

39 We performed experimental range expansions in an aquatic model system, with natural dispersal of

40 infected hosts. Parasites from experimental range fronts were less virulent and interfered less with host

41 dispersal, but also invested less in horizontal transmission than parasites from the range core. Thus,

42 dispersal adaptation at the front may come at a cost of reduced horizontal transmission, a trade-off rarely

43 considered in theoretical models on parasite virulence evolution. These results have important

44 implications in the context of emerging diseases, and for parasite evolution during biological invasions

45 or other spatial non-equilibrium scenarios.

46

47 **INTRODUCTION**

48 In an increasingly connected world, and with changing environments and habitats, we are facing the risk

49 of infectious diseases spreading outside their natural range and over large geographic scales (1–5). This

50 issue is of concern to human health, agriculture and wildlife conservation, and understanding the

51 ecological and evolutionary drivers represents a major challenge to epidemiologists and evolutionary

52 biologists (6–8). Due to their short generation time and large population sizes, parasites have the

53 potential to evolve rapidly, and therefore one important question is whether changes in transmissibility

54 or virulence already occur while an epidemic is progressing (9). Classic theory predicts evolutionary

55 optima for these traits only in large, spatially homogeneous populations at equilibrium (10, 11), but

56 these conditions are unlikely to be met during an epidemic (12, 13). In patchy real-world populations,

57 parasites experience extinction-recolonization dynamics typical of metapopulations, with epidemic

58 spread critically depending on population connectivity and the mobility and dispersal of infected hosts

59 (14–19). Although fundamental for epidemiology, it is still unclear how these spatio-temporal aspects

60 affect concomitant evolutionary processes, and whether they might even lead to specific parasitic

61 adaptations enhancing the spatial spread of the epidemic (see 20–22)

62 Recent theory has begun to develop a conceptual framework to investigate parasite evolution in spatially

63 explicit, non-equilibrium settings (23). Assuming a classic virulence-transmission trade-off (24, 25) and

64 local feedbacks between epidemiology and selection, several models predict that more virulent parasites

65 will evolve in highly connected "small-world" landscapes (26–28) or at the front of advancing epidemics

66 (20), where host exploitation and transmission is not limited by local depletion of susceptible hosts

67 ("self-shading"). These predictions are consistent with observed changes in the predominance of a

68 highly virulent honeybee virus at the front of progressing epidemics in New Zealand (29), and

69 potentially also with observations for parasites and pathogens of amphibian species (30, 31).

70 Yet, not all host-parasite systems show this pattern. For instance, the geographic spread of a bacterial

71 pathogen of North American house finches was associated with decreased virulence in the newly

72 invaded areas (32). Likewise, in monarch butterflies, hosts that sustain long or frequent migrations were

73 found to harbour less virulent parasites (33). This may be explained by the way parasite dispersal enters

4

74   into the equation. Namely, if parasites travel with their infected hosts, exploitation of host resources

75   may reduce dispersal, thereby introducing a novel dispersal-virulence trade-off. Osnas et al. (2015) (22)

76   show that such trade-off can lead to selection favouring more prudent and dispersal-friendly parasites

77   at the moving edge of an epidemic that escape more virulent and transmissible parasites from the core

78   of an epidemic. This latter idea mirrors classic principles from metapopulation theory and

79   metacommunity ecology, based on trade-offs between competitive ability and colonisation/dispersal

80   (20, 34–36). It also relates to recent work on invasive species and range expansions, where dispersal

81   evolution plays a key role in determining the rate of spatial diffusion (37). In this sense, parasites may

82   evolve 'invasion syndromes', with characteristic changes in morphology, life history or transmission

83   strategies (30, 31, 38), thereby creating a positive feedback loop between rates of dispersal and rates of

84   spatial spread of infection.

85   Although the study of naturally expanding parasites remains the ultimate litmus test of the theory,

86   controlled experiments can verify important assumptions and serve as proof of principle (39). For

87   example, we can manipulate demographic conditions in experimental microcosms to mimic the front

88   and core of an expanding epidemic (36) or artificially change levels of population mixing to study

89   epidemiological or evolutionary processes (39). Indeed, studies of the latter type found that

90   experimentally shifting populations from local to global "dispersal" favoured more virulent parasites

91   (40–42), as predicted by theory (23, 43). Yin (1993) (44) further showed that phage diffusion on

92   bacterial lawns is associated with the appearance of faster replicating mutants in the periphery. However,

93   to our knowledge, there are no studies addressing experimental evolution of parasites from an explicit

94   metapopulation perspective, under natural dispersal of a host and its parasite.

95   For (micro-)organisms with directed movement, experimental landscapes can be created to study

96   metapopulation processes or range expansion dynamics with natural dispersal (45–47). Here, we

97   employed such an approach to investigate the experimental evolution of spatially spreading parasites,

98   where all parasite dispersal is host-mediated. Using two-patch dispersal arenas for the ciliate

99   *Paramecium caudatum* infected with the bacterial parasite *Holospora undulata*, we mimicked a range

100   expansion scenario, with a front population of hosts (and parasites) dispersing into a new microcosm

5

101 during each selection event, and a core population constantly remaining in place (and losing emigrants;

102 see Fig. 1). After 55 episodes of dispersal selection, we then assayed evolved front and core parasites

103 under common garden conditions on naive hosts. Multiple traits were measured, namely the parasites'

104 effect on host dispersal, investment in horizontal transmission and their impact on host replication and

105 survival. We further obtained additional independent estimates of parasite traits by fitting a simple

106 epidemiological model to time series data (population density, infection prevalence) from the

107 experimental assay.

108 Because parasite persistence in the front populations depended entirely on host dispersal, we predicted

109 that front parasites would evolve minimal impact on host dispersal, or even increase dispersal of infected

110 hosts (48). Such dispersal adaptations could involve a decrease in parasite virulence (22) and generate

111 an evolutionary trade-off with investment in horizontal transmission, not expected to occur in the core

112 populations. Our results were broadly consistent with these predictions, and we conclude that

113 differential dispersal selection pressures arising at the core and front of a range expansion can lead to

114 marked divergence of parasite life-history traits and the emergence of a 'parasite dispersal syndrome'.

115 **RESULTS**

116 Evolved parasites from the five front and five core selection lines were extracted and the inocula used

117 to infect naïve hosts (three genotypes). Several traits were measured for these newly infected assay

118 cultures (for timing of assays see Table S1 and statistical analyses Tables S2, S3).

119 **Infected host dispersal**

120 On average, hosts infected with front parasites dispersed twice as much (mean dispersal rate: $0.24 \pm$

121 0.05 SE x $3h_{-1}$) as those infected with the core parasites (0.12 ± 0.02 SE; Fig. 2A). This effect of selection

122 treatment was significant ($\chi_{12} = 4.9$, p = 0.027; Table S2). The distribution of the differences between

123 model predictions for front and core treatments (small panel, Fig. 2A) also shows that higher front-

124 parasite dispersal is the most frequent predicted outcome (>98%; mean front-core difference: 0.12, 95%

125 CI [0.08; 0.35]). This general trend was consistent on all three host genotypes tested (Fig. S4; Table S3).

126 Fig. S4 further shows that levels of front-parasite dispersal were similar to reference data for uninfected

127 hosts, whereas core parasites generally reduced dispersal.

6

128   Using video analysis, we investigated variation in two parameters of *Paramecium* swimming behaviour:

129   swimming speed and trajectory variation (tortuosity). We found no evidence that infection with core or

130   front parasites had significant effects on these two parameters ($p > 0.25$; Table S2, neither when tested

131   on host genotypes individually S3; Fig S5, S6). Moreover, mean levels of swimming speed or tortuosity

132   were not significantly correlated with infected dispersal rates ($r \leq 0.15$, $n = 29$, $p > 0.4$), indicating that

133   dispersal was not directly affected by these aspects of swimming behaviour (see also path analysis

134   below).

135   **Parasite life-history traits**

136   **Infectivity.** Measurements of infection prevalence early after inoculation (day 4) inform on parasite

137   horizontal transmission potential (infectivity). Core parasites had slightly higher infection success

138   (selection line average proportion of infected hosts: 0.59 ± 0.05 SE) than front parasites (0.51 ± 0.03

139   SE; Fig. 2B). Although not formally significant (effect of selection treatment: $\chi_{12} = 2.43$, $p = 0.118$;

140   Table S2; predictive difference distribution front-core infectivity: mean = -0.08, CI [0.02; -0.18]; Fig

141   2B; see also Fig. S7 for genotype specific responses), this trend was consistent with higher estimates of

142   the transmission parameter for core parasites in an epidemiological model fitted to our experimental

143   data (see below; Fig. 4).

144   **Investment in horizontal transmission (infectiousness).** It takes several days until infected hosts

145   produce horizontal transmission stages and become infectious. In our assay, the first infectious hosts

146   appeared on day 6 p.i., and their frequency then increased over the following week, reaching up to 100%

147   (Fig. 2C). Over this period, populations infected with front parasites produced a lower proportion of

148   infectious hosts (mean: 0.41 ± 0.03 SE) than did populations infected with core parasites (0.53 ± 0.03

149   SE; effect of selection treatment: $\chi_{12} = 13.2$, $p < 0.001$; Table S2; predictive difference distribution front-

150   core infectiousness: mean = -0.10; CI [0.04; -0.23]; Fig. 2C). There was also a difference in timing: on

151   average, core parasites produced the first infectious hosts c. 1 day earlier than did front parasites (day 6

152   vs day 7) and subsequently showed a faster increase in the proportion of infectious hosts (treatment x

153   time interaction: $\chi_{12} = 13.54$, $p < 0.001$, Table S2; Fig. 2C). These differences in total investment and/or

154   timing broadly hold on all three host genotypes tested (Table S3; Fig. S8).

7

155   **Virulence.** We isolated single infected individuals from the core and front infected assay cultures and

156   measured the impact of infection on host division and survival over a 20-day period. Exposed, but

157   uninfected, controls were isolated from the same assay cultures and run in parallel.

158   *Host division.* By day 10, 87% of the infected singletons had accomplished at least one division (266 /

159   305 replicates; mean maximum cell number observed over this period: 8.5 ± 0.6 SE). Analysis of

160   maximum cell density revealed a significant selection treatment x infection status interaction ($\chi_{12} = 16.9$,

161    $p > 0.001$; Table S2). Namely, hosts infected with front parasites reached nearly twice as high maximum

162   densities (10.9 ± 1.3 SE) than those infected with core parasites (5.9 ± 0.9 SE; contrast front vs core:

163    $t_{601} = 4.7$, $p < 0.0001$; predictive difference distribution front-core: mean = 4.6, CI [1.4; 9.6]; Fig. 3A).

164   *Host survival.* As for host division, there was a significant selection treatment x infection status

165   interaction for host survival ($\chi_{12} = 7.4$, $p = 0.006$; Table S2). By day 20, infections with front parasites

166   had experienced a 50% lower mortality (mean proportion of infected replicates extinct: 0.19 ± 0.05 SE)

167   than infections with core parasites (0.37 ± 0.1 SE; contrast front vs core: $t_{601} = 3.75$, $p > 0.001$; predictive

168   difference distribution front-core: mean = 0.30, CI [0.04;0.62]; Fig. 3B). Moreover, effects on host

169   division and on host survival were positively correlated: parasites which allowed more host division

170   also allowed higher host survival (means per parasite selection line: $r = 0.84 \pm 0.19$, n = 10, $p = 0.003$).

171   Thus, core parasites generally had negative effects, whereas front parasites only had little, or even

172   positive, impact on their hosts reproduction and survival (Fig. 3A and 3B), and these opposing trends

173   were consistent across the three host genotypes tested (Table S2; Fig. S9 & S10).

174   **Path analysis**

175   Using path analysis, we explored the direct and indirect contributions of different traits to the observed

176   variation in infected host dispersal (Fig. 4A). Host division (= maximum cell density) was the only trait

177   with a significant direct effect on host dispersal ($F_{1,20} = 6.16$, $p = 0.022$; Fig. 3B); thus, lower virulence

178   was associated with higher dispersal rates of infected hosts. Horizontal transmission investment (=

179   cumulative infectiousness) had a moderate indirect effect on dispersal via its significant negative

180   relationship with virulence ($F_{1,23} = 4.47$, $p = 0.0456$; Fig. 3C). Swimming behaviour (speed, tortuosity)

181   had no significant direct effect on dispersal, and were themselves only very marginally affected by

182   virulence or infectiousness (Fig. 4A).

183   **Epidemiological model fits**

184   By fitting an epidemiological model to the population-level data from the assay replicate cultures

185   (infection prevalence and population density), we obtained independent estimates of parasite

186   parameters. In the model, we integrated the basic features of the infection life cycle, assuming simple

187   population growth and regulation (Beverton-Holt type model, 49) and parameterising virulence as the

188   reduction in host fecundity.

189   The model captured the main trends in the demographic and epidemiological dynamics observed in the

190   cultures. This is illustrated in Fig. 5A, showing the model fits for the densities of infected and uninfected

191   hosts for the 63D host genotype (for the other two host genotypes, see SI 4, Fig. S11). Parameter

192   estimates confirm the main trends found in our experimental assays. Namely, the model fits show that

193   front parasites have lower virulence, lower transmission rate and longer latency time than core parasites

194   (Fig. 5B-D), a pattern largely consistent for the three host genotypes tested (Fig. S11).

195   **DISCUSSION**

196   In times of global epidemics (1, 4, 32) it is important to know how parasites evolve while spreading

197   through a landscape or entire continents. Recent theory suggests that spatial 'viscosity' and

198   connectedness generate eco-evolutionary feedbacks, with important consequences for parasite virulence

199   evolution and the speed of epidemics (23). However, so far little attention has been given to the fact

200   that many parasites travel together with their dispersing hosts, which may considerably affect

201   evolutionary predictions (28, 50, 51).

202   To address this issue, we performed a simplified range expansion experiment, with natural dispersal of

203   infected hosts. Our 'range front' and 'range core' treatments imposed differential selection on host

204   dispersal (see 52) and resulted in divergent parasite phenotypes: front parasites allowed for higher

205   dispersal of their infected hosts, were less virulent and showed reduced investment in horizontal

206   transmission, compared to the parasites from the core selection treatment. These patterns were largely

9

207   robust between the three naive host genotypes tested, and additionally confirmed by results from an

208   epidemiological model that we fitted to time-series data obtained from our assay cultures.

209   *Evidence for a virulence - dispersal trade-off*

210   Our experimental result of multi-trait changes joins empirical observations of "invasion syndromes" in

211   naturally spreading diseases, such as avian malaria in Europe (53) or lungworms of invasive cane toads

212   in Australia (30). Lungworms at the invasion front, for example, exhibit distinct life-history traits

213   (reduced age at maturity, larger infective and free-living larvae), possibly representing adaptations to

214   invasion history (30). We replayed such an invasion history, by mimicking the spatial progression of an

215   isolated population in our range front treatment, which was expected to favour parasites that succeed in

216   dispersing together with their infected hosts. This explains why our front parasites were found to

217   facilitate higher host dispersal. Importantly, higher host dispersal was associated with higher host

218   replication and survival, indicating a dispersal - virulence trade-off (Fig. 2 and 3). Reduced virulence,

219   in turn, was associated with reduced horizontal transmission potential (Fig. 2C), consistent with previous

220   findings in this system (54–56) and reflects a virulence-transmission trade-off for this parasite. Thus,

221   we conclude that the evolution of higher parasite dispersal in front parasites came at the cost of reduced

222   horizontal transmission, a trade-off resulting from a reduction in virulence.

223   The idea that parasite exploitation strategies can be shaped by the interplay between local transmission

224   and global dispersal was formalised in a theoretical model by Osnas et al. (2015) (22). They showed

225   that implementing a trade-off between virulence and the capacity of infected hosts to disperse, favours

226   less virulent strains at the front of an epidemic, escaping the more competitive (and more virulent) strains

227   through faster dispersal (22). Such a selection scenario may explain observed geographic patterns of

228   virulence for a bacterial pathogen of North American house finches (32), and it is qualitatively consistent

229   with our results.

230   *Trait relationships: Proximate causes of infected dispersal rate*

231   Just like parasites can alter their hosts behaviour to increase transmission (57), they may also evolve to

232   manipulate host dispersal (50, 58). However, we find little evidence for manipulation to increase the

233   dispersal. Consistent with previous observations of negative effects of infection in this (59) and other

10

234   systems (36, 60–62), core parasites reduced host dispersal, whereas infection with front parasites

235   produced levels of dispersal comparable to uninfected *Paramecium*. Path analysis indicates that

236   virulence is the main direct predictor of host dispersal in our assays. Investment in horizontal

237   transmission had an indirect effect via decreased virulence. Although intuitively straightforward through

238   a weakening of infected hosts, the mechanistic link between virulence and dispersal remains unclear.

239   We found no effect of infection on swimming behaviour, nor was there a direct link between swimming

240   behaviour and dispersal, which is frequently observed in other protists (63). Possibly, infection

241   influences other dispersal-relevant traits, such as the vertical distribution in the water column (64, 65),

242   determining the proximity of individuals to the opening that leads to the other tube in the dispersal arena

243   (see Fig. 1).

Contrasting scenarios: Dispersal to new sites vs access to new hosts

245   While our results suggest more prudent parasites might be spreading at invasion fronts, other theoretical

246   models and experiments reach opposite conclusions. Griette et al. (2015) (21), for example, predict

247   highest levels of virulence at the front of an epidemic wave, where transmission is not limited by the

248   availability of susceptible hosts, thereby favouring the most 'rapacious' variants. Following this line of

249   argument, experiments with viruses and bacteriophages have studied virulence evolution by artificially

250   manipulating dispersal or population connectivity (40–42). Kerr et al. (2006) pipetted bacteria and phage

251   either to adjacent wells or to more distant wells on a multi-well plate, in analogy to our 'core' and 'front'

252   treatments (41). Contrary to our results, their latter treatment of unrestricted dispersal resulted in the

253   evolution of more virulent phages, confirming the prediction that erosion of spatial structure in 'small

254   worlds' favours more transmissible and more virulent parasites (27, 28, 66).

255   One reason for these contrasting results is that in Kerr et al. (2006) (41), dispersal was artificial and

256   cost-free, eliminating a possible virulence-dispersal trade-off. Secondly, our experiment considered a

257   different spatial scenario where infected hosts disperse into empty space, more characteristic of a

258   biological invasion. This means that higher dispersal was not rewarded with more access to susceptible

259   hosts, as assumed in the above models (20, 66). Future experiments can test whether we still find reduced

11

260　virulence in the front selection treatment, if infected hosts disperse into patches already occupied by

261　uninfected hosts.

262　Taken together, these examples illustrate the different ways in which spatial spread and dispersal of

263　parasites can be approached both conceptually and experimentally, with very different evolutionary

264　outcomes. We argue that particular attention should be given to *how* parasites disperse through a

265　landscape, namely because dispersal itself may be the target of selection (36, 51).

266　**More vertical transmission at invasion fronts?**

267　We used the replication of infected hosts as a measure of virulence. However, for this parasite, host

268　replication is also equivalent to vertical transmission, because reproductive stages are passed on to

269　daughter cells during mitosis. In this sense, parasites in our front selection treatment underwent a shift

270　from horizontal transmission towards higher levels of vertical transmission. This is due to an underlying

271　developmental trade-off, where reduced conversion of reproductive into infective stages decreases the

272　negative effects on host replication (56, 67), but simultaneously reduces horizontal transmission

273　capacity.

274　Magalon et al. (2010) observed a similar increase in the efficacy of vertical transmission of this parasite

275　in frequently disturbed populations (55). In fact, their study can be re-interpreted as a range expansion

276　experiment, with the disturbance treatment mimicking the frequent recolonization events occurring at

277　the front (68) and the less disturbed control treatment reflecting more stable conditions in the core (see

278　Fig. 1 in 55). The explanation for the evolutionary shift towards vertical transmission is that the

279　demographic oscillations at the invasion front, with frequent periods of low host density and high host

280　fecundity, increase the contribution of vertical transmission to the total transmission success (69).

281　Because vertical transmission is a means of 'reproductive insurance', we would generally expect it to

282　evolve in association with parasite dispersal syndromes in expanding populations or in highly disturbed

283　habitats (70). We note, however, that in our present experiment both core and front populations went

284　through density bottlenecks, making the dispersal constraint the main selective driver.

285　**Conclusions**

286   Our results show that different segments of an epidemic wave may be under divergent selection

287   pressures. Namely, we find evidence that dispersal selection at an experimental invasion front leads to

288   reduced virulence. This contrasts with observations in certain natural epidemics (29, 30), while

289   confirming others (32, 33). This calls for more detailed investigations of the role of dispersal for

290   epidemic spread and its implications for the evolution of parasite life-history traits. Our relatively simple

291   statistical modelling exercise suggests that time series data from natural populations represent a useful

292   resource for such a challenge. Establishing a better understanding of the interaction between

293   demography and rapid evolutionary change in spreading populations is crucial for the management of

294   emerging infectious diseases and disease outbreak in the wild, biological invasions and other non-

295   equilibrium scenarios.

296

297   **MATERIALS AND METHODS**

298   *Study system*

299   *Paramecium caudatum* is a filter-feeding freshwater protozoan ciliate from still water bodies in the

300   Northern Hemisphere (71). It has a germline micronucleus and a somatic macronucleus. Our cultures

301   are maintained asexually in a lettuce medium with the food bacterium *Serratia marcescen*s at 23°C,

302   allowing 1-2 population doublings per day (72). The gram-negative alpha-proteobacterium *Holospora*

303   *undulata* infects the micronucleus of *P. caudatum*, and can be transmitted both horizontally (by s-shaped

304   infective spores, 15 µm) upon host death or during cell division, and vertically, when reproductive

305   bacterial forms (5 µm) segregate into daughter nuclei of a mitotically dividing host (73). After ingestion

306   by feeding *Paramecium,* infective spores invade the micronucleus, where they differentiate into the

307   multiplying reproductive forms. After one week, reproductive forms begin to differentiate into infective

308   spores (64, 72). Infection with *H. undulata* reduces host cell division and survival (56) and also host

309   dispersal (59).

310   *Long-term experiment*

311   Similar to Fronhofer and Altermatt (2015), we imposed dispersal selection in 2-patch microcosm arenas

312   (Fig. 1, see also SI 1), built from two 14-mL plastic tubes, interconnected by 5-cm silicon tubing, which

313   can be blocked using a clamp (see Fig. S1). We define dispersal as the active swimming of *Paramecium*

314   from one microcosm to the other via the connective tuber (i.e., the dispersal corridor).

315   The experiment was seeded from an uninfected host line ("63D", haplotype b05) from our laboratory

316   that had been under "core selection" (see below) for three years and shows characteristically low

317   dispersal propensity (O.K., unpublished data). This 63D mass culture was infected with an inoculum of

318   *H. undulata* prepared from a mix of various infected stock cultures (for details, see SI 2). All parasites

319   in this mix originate from a single isolate of *H. undulata* established in the lab in 2001.

320   In the front selection treatment, we placed *Paramecium* in one tube ("core patch") and opened the

321   connection for three hours, allowing them to swim into the other tube ("front patch"). *Paramecium* from

322   the front patch were recovered and cultured in bacterised medium, allowing for natural host population

323   growth and parasite transmission. After one week, we imposed another dispersal episode, again

324   recovering only the *Paramecium* from the front patch, and so on. The core selection treatment followed

325   the same alternation of dispersal and growth periods, except that only *Paramecium* from the core patch

326   were recovered and propagated (Fig. 1, and SI 1). We established five infected 'core selection' lines and

327   five infected 'front selection' lines that were maintained for a total of 55 cycles of dispersal. To minimise

328   potential effects of host (co)evolution, we extracted infectious forms from each selection line after cycle

329   30, inoculated a new batch of naïve 63D hosts and continued the experiment for another 25 cycles. For

330   details of the experimental protocols, see SI 1.

331   *Parasite assays*

332   At the end of the selection experiment, we extracted parasites from core and front selection lines to

333   inoculate new, naïve hosts. We then assayed parasite effects on host dispersal, infection life-history and

334   virulence. To obtain a general picture of trait expression, we tested the evolved parasites on naïve 63D

335   hosts (same genotype as used in long-term experiment), as well as on two other genotypes, C023 and

336   C173 (provided by S. Krenek, TU Dresden, Germany). Companion assays of evolutionary adaptations

337   arising in the host are reported elsewhere (52).

14

338   All assays were performed on a cohort of infected replicate cultures, over the course of three weeks

339   under common-garden conditions (Table S1). To initiate the cultures, we placed ≈ 5 x 10_3 cells of a

340   given naïve host genotype in 1.4 mL of bacterised medium in a 15-mL tube, to which we added the

341   freshly prepared inoculum of a given evolved parasite line (≈ 1.5 x 10_6 infectious spores, on average).

342   On day four post-inoculation (p.i.), when infections had established, we split the cultures into three

343   technical replicates and expanded the volume to 30 mL, by adding bacterised medium. A total of 90

344   replicate cultures were set up (2 selection treatments x 5 parasite selection lines x 3 host genotypes 3

345   technical replicates).

Dispersal of infected hosts

347   From day 14 to 19 p.i., we assayed dispersal rates of hosts infected with core and front parasites, using

348   linear 3-patch arenas where the *Paramecium* disperse from the middle tube to the two outer tubes (Fig.

349   S2). Arenas were filled with ~2800 individuals in the middle tube and after 3 h of dispersal, we

350   subsampled the middle tube (0.5 mL) and the pooled two outer tubes (3 mL) to estimate the number of

351   non-dispersers and dispersers under a dissecting microscope. Furthermore, from ≈20 arbitrarily picked

352   individuals stained with 1% lacto-aceto orcein (LAO fixation; Fokin and Görtz, 2009) we determined

353   the proportion of infected dispersers and non-dispersers (phase-contrast, 1000x magnification), from

354   which we then calculated the dispersal rate of infected hosts for each replicate culture (number of

355   dispersed infected hosts / total number of infected hosts per 3 h). Each of 88 available replicate cultures

356   was tested once. For statistical analysis, we excluded 13 replicates with very low population density

357   and/or infection prevalence (<10%), which prevented accurate estimation of dispersal of infected

358   individuals. Dispersal was not significantly affected by assay date (χ_{22} = 2.56, p > 0.25), and this factor

359   was therefore omitted from further analysis.

Parasite life-history traits

361   Infectivity. On day 4 p.i., we estimated infection prevalence in the 30 inoculated cultures, using LAO

362   fixation of ≈20 individuals, as described above. This measurement describes 'parasite infectivity', i.e.,

363   the capacity to successfully establish infections (64).

15

364 Epidemiology and parasite development. From day 6 to 13 p.i., we tracked population density and

365 infection prevalence in the 90 replicate cultures, using a blocked sliding window (day 6-8, 11-13) such

366 that each parasite x host genotype combination was measured once per day. As infections developed,

367 we also tracked changes in the proportion of infectious hosts, when reproductive forms are converted

368 into infective spores. These data were used for the fitting of an epidemiological model (see below).

369 Furthermore, we specifically compared core and front parasites for their levels of infectiousness (=

370 proportion of infectious hosts) between day 6 and day 11 p.i.. This time window describes the timing

371 and level of investment into horizontal transmission by the initial cohort of infected hosts (72).

372 Virulence. Early after inoculation of the initial 30 assay cultures (day 4 p.i.), we isolated single infected

373 and uninfected individuals from each culture and let them multiply for 9 days in 2-mL tubes under

374 permissive common-garden conditions. From these small monoclonal cultures, we started the virulence

375 assay by placing single individuals in PCR tubes filled with 200 μL of medium. We assessed cell

376 division on day 2 and 3 (visual inspection), on day 10 (from 50-μL samples) and on day 20 from the

377 total volume. A total of 645 replicates were set up, with 8-12 infected and uninfected replicates from

378 each of 28 of the 30 assay cultures. For further details, see SI 2 and Fig. S3.

379 Swimming behaviour. From the above monoclonal lines, we placed 200-μL samples (containing 10-20

380 individuals) on a microscope slide and recorded individual movement trajectories using a Perfex

381 SC38800 camera (15 frames per second; duration 10 s). For each sample, the mean net swimming speed

382 and swimming tortuosity (standard deviation of the turning angle distribution, describing the extent of

383 swimming trajectory change) was determined, using the BEMOVI package (75). This assay was

384 performed for infected and uninfected monoclonal lines from 29 assay cultures, with 1-2 samples per

385 monoclonal line (106 replicates in total).

386 ***Statistical analysis***

387 Statistical analyses were performed in R (ver. 3.3.3; R Development Core Team, available at www.r-

388 project.org) and in JMP (SAS Institute Inc. (2018) JMP®, Version 14, N.C.). To analyse variation in

389 parasite traits, we used generalised linear mixed-effect models (76). Binomial error structure and logit

16

390   link were used for analysis of infected host dispersal (proportion dispersers), infectivity (proportion

391   infected individuals on day 4 p.i.), and horizontal transmission investment (proportion infectious hosts

392   day 6-11 p.i.). Normal error structure was used for analysis of swimming speed and tortuosity. For the

393   virulence assay, we analysed variation in host division (= maximum cell density per replicate; Poisson

394   error structure and log link) and survival (= replicate alive / dead on day 20; binomial error structure

395   and logit link).

396   In all analyses, parasite selection treatment (front vs core) was taken as a fixed effect and host genotype

397   and parasite selection line identity as random factors. Day p.i. was integrated as a covariate in the

398   analysis of infectiousness. In the virulence analyses, replicate infection status (infected / uninfected)

399   was included as a fixed factor. Analysis of variance (type II) was used to test for significance of fixed

400   effects (car package; Fox and Weisberg, 2018). In complementary comparisons, we used ANOVA

401   model predictions (and their variance) for core and front treatments to establish predictive distributions

402   of the front-core difference (e.g. Fronhofer *et al.*, 2017). For these distributions, we calculated the mean

403   difference and confidence intervals. Finally, we performed multiple regressions (path analysis) to assess

404   how infected host dispersal was affected by the following traits: horizontal transmission investment

405   (HTI, area under the curve of the proportion of infectious hosts from day 6 - 11 p.i.), virulence (infected

406   host division) and swimming behaviour (tortuosity and net swimming speed). This analysis was based

407   on trait means for 25 combinations of parasite selection line and host assay genotype. To meet

408   assumptions of normality, certain trait means were transformed (log_2 for host division, arcsine for

409   dispersal, square root for HTI). To correct for overall effects of host genotype, we first fitted univariate

410   analyses for each trait, and then performed the regressions on the residuals. Standardised beta regression

411   coefficients were taken as path coefficients.

Epidemiological model fitting

413   We fitted a simple epidemiological model to the above population density and infection prevalence data

414   recorded in our assay replicate cultures (day 6-13 p.i.). The aim was to obtain additional independent

415   estimates of parasite parameters (Table 1), namely virulence, but also the transmission parameter or

416   latency time, i.e. the time to onset of production of infectious forms (Rosenbaum et al., 2019).

17

417   <u>Model structure</u>. We model the density of uninfected (S) and infected (I) hosts using ordinary differential

418   equations (ODEs). In the absence of parasites, we consider that uninfected *Paramecium* growth follows

419   the continuous time version of the Beverton-Holt model (49).

420     $\frac{dS}{dT} = \left(\frac{b}{1+\alpha N} - d \right) S$ (1)

421   where b is the birth rate, d the death rate and α the competition term. N is the total number of individuals

422   ($S + I$), which is equal to S in the absence of the parasite. In the presence of infected individuals,

423   uninfected individuals become infected at a rate proportional to the number of infected and uninfected

424   individuals at a rate β:

425     $\frac{dS}{dT} = \left(\frac{b}{1+\alpha N} - d \right) S - \beta SI$ (2)

426     $\frac{dI}{dT} = \beta SI$ (3)

427   Moreover, infected individuals also display Beverton-Holt dynamics, but their birth rate can be

428   decreased, hence we multiply b by a term $(1 - v)$, where v is the virulence of the parasite:

429     $\frac{dS}{dT} = \left(\frac{b}{1+\alpha N} - d \right) S + \beta SI$ (4)

430     $\frac{dI}{dT} = \left(\frac{b(1-v)}{1+\alpha N} - d \right) I + \beta SI$ (5)

431   Finally, vertical transmission of the parasite is not necessarily 100%, and some of the *Paramecium*

432   "born" from infected individuals could be free of parasites due to incomplete vertical transmission. We

433   name γ the proportion of successful vertical transmission:

434     $\frac{dS}{dT} = \left(\frac{b}{1+\alpha N} - d \right) S - \beta SI + \left(\frac{b(1-v)}{1+\alpha N} \gamma \right) I$ (6)

435     $\frac{dI}{dT} = \left(\frac{b(1-v)}{1+\alpha N} \gamma - d \right) I + \beta SI$ (7)

436   Since the majority of infected individuals were not yet producing infectious forms at the beginning of

437   the time series, we added another parameter, τ, which is the latency before an infected individual

438   becomes infectious (i.e., capable of horizontal transmission):

439     $\beta = 0 \; if \; time < \tau$ (8)

440   <u>Model Fitting</u>. We fitted the epidemiological model to the data using Bayesian inference and the *rstan*

441   R package (version 2.19.2). Using data from previous experiments (O. Kaltz, unpublished data), we first

442   fitted the Beverton-Holt model (Eq. 1) to growth curves of uninfected populations to estimate the

443   distributions of *b, d* and *α* for each host genotype. These distributions were used as priors for fitting the

444   full model (Eq. 6, 7, 8) on infection data. The model was fitted separately for each of the six

445   combinations of host genotype and parasite selection treatment. For simplicity, we fitted a single set of

446   parameters (*b, d, α, b, β, γ, τ*) over the different selection lines (with different initial conditions fitted

447   over each line). Priors distributions can be found in Table 1. Apart from *b,* d and α, we used lowly

448   informative priors that largely encompass expected values (*v* and *γ* priors are uniform over possible

449   values, *τ* prior is uniform over previously observed latency values, *β* prior follows a lognormal

450   distribution an order of magnitude wider than expected values). Fits were realized using the No U-Turn

451   Sampler (NUTS) with default rstan values and multiple chains (three chains per fit, each of total length:

452   15 000 and warm-up length: 5 000).

453   **Table 1**. Model parameters, their signification and the priors used for fitting.

Parameters	Term	Priors
b	Birth rate	Posteriors from fitting eq. (1) on non-infected population data
d	Death rate	
α	Intraspecific competition coefficient	
v	Virulence (decrease in b)	Uniform (0, 1)
β	Horizontal transmission rate	Lognormal (-5, 0.9)
γ	Vertical transmission rate	Uniform (0.5, 1)
τ	Latency time	Uniform (144, 240)

454

Acknowledgements

19

Author contributions

OK, LN and GZ conceived the study. OK, LN, GZ, MH, and EAF helped design the experiments. LN, GZ, CGB and OK performed the experimental work., LN, GZ, MH, OK and EAF performed the statistical analysis. EAF, CS and OK developed, and CS analysed the epidemiological model. All authors interpreted the results and contributed to the writing of the manuscript.

Data accessibility

If the manuscript is successfully accepted for publication, data will be available at Dryad or Figshare.

REFERENCES

1. J. Bahl, *et al.*, Temporally structured metapopulation dynamics and persistence of influenza A H3N2 virus in humans. *Proc. Natl. Acad. Sci. U. S. A.* **108**, 19359–19364 (2011).

2. J. H. O. Pettersson, *et al.*, Re-visiting the evolution, dispersal and epidemiology of Zika virus in Asia article. *Emerg. Microbes Infect.* **7**, 1–8 (2018).

3. A. Findlater, I. I. Bogoch, Human mobility and the global spread of infectious diseases: a focus on air travel. *Trends Parasitol.* **34**, 772–783 (2018).

4. M. Chinazzi, *et al.*, The effect of travel restrictions on the spread of the 2019 novel coronavirus (COVID-19) outbreak. *Proc. 20th USENIX Secur. Symp.* **6 March**, 395–410 (2020).

5. A. J. Tatem, D. J. Rogers, S. I. Hay, Global transport networks and infectious disease spread. *Adv. Parasitol.* **62**, 293–343 (2006).

6. S. R. Parratt, E. Numminen, A.-L. Laine, Infectious disease dynamics in heterogeneous landscapes. *Annu. Rev. Ecol. Evol. Syst.* **47**, 283–306 (2016).

7. R. M. Penczykowski, A. L. Laine, B. Koskella, Understanding the ecology and

483   evolution of host-parasite interactions across scales. *Evol. Appl.* **9**, 37–52 (2016).

484   8.   N. J. Clark, *et al.*, Climate, host phylogeny and the connectivity of host communities

485   govern regional parasite assembly. *Divers. Distrib.* **24**, 13–23 (2018).

486   9.   E. C. Holmes, G. Dudas, A. Rambaut, K. G. Andersen, The evolution of Ebola virus:

487   Insights from the 2013-2016 epidemic. *Nature* **538**, 193–200 (2016).

488   10.   C. E. Cressler, D. V. McLeod, C. Rozins, J. Van Den Hoogen, T. Day, The adaptive

489   evolution of virulence: a review of theoretical predictions and empirical tests.

490   *Parasitology* **143**, 915–930 (2016).

491   11.   S. Alizon, A. Hurford, N. Mideo, M. Van Baalen, Virulence evolution and the trade-off

492   hypothesis: History, current state of affairs and the future. *J. Evol. Biol.* **22**, 245–259

493   (2009).

494   12.   J.-B. Andre, M. E. Hochberg, Virulence evolution in emerging infectious diseases.

495   *Evolution (N. Y).* **59**, 1406–1412 (2005).

496   13.   S. Gandon, T. Day, Evolutionary Epidemiology and the Dynamics of Adaptation.

497   *Evolution (N. Y).* **63**, 826–838 (2009).

498   14.   M. J. Keeling, *et al.*, Dynamics of the 2001 UK Foot and Mouth epidemic: Stochastic

499   dispersal in a heterogeneous landscape. *Sci. New Ser.* **294**, 813–817 (2001).

500   15.   C. Viboud, *et al.*, Synchrony, waves, and spatial hierarchies in the spread of influenza.

501   *Science (80-.).* **312**, 447–451 (2006).

502   16.   G. Dudas, *et al.*, Virus genomes reveal factors that spread and sustained Ebola

503   epidemic. *Physiol. Behav.* **544**, 309–315 (2017).

504   17.   M. J. Ferrari, *et al.*, The dynamics of measles in sub-Saharan Africa. *Nature* **451**, 679–

505   684 (2008).

21

506 18. A. R. North, H. C. J. Godfray, The dynamics of disease in a metapopulation: The role

507   of dispersal range. *J. Theor. Biol.* **418**, 57–65 (2017).

508 19. J. Jousimo, *et al.*, Ecological and evolutionary effects of fragmentation on infectious

509   disease dynamics. *Science (80-.).* **344**, 1289–1293 (2014).

510 20. Q. Griette, G. Raoul, S. Gandon, Virulence evolution at the front line of spreading

511   epidemics. *Evolution (N. Y).* **69**, 2810–2819 (2015).

512 21. G. E. Leventhal, A. L. Hill, M. A. Nowak, S. Bonhoeffer, Evolution and emergence of

513   infectious diseases in theoretical and real-world networks. *Nat. Commun.* **6** (2015).

514 22. E. E. Osnas, P. J. Hurtado, A. P. Dobson, Evolution of pathogen virulence across space

515   during an epidemic. *Am. Nat.* **185**, 332–342 (2015).

516 23. S. Lion, S. Gandon, Evolution of spatially structured host-parasite interactions. *J. Evol.*

517   *Biol.* **28**, 10–28 (2015).

518 24. J. J. Bull, Virulence. *Evolution (N. Y).* **48**, 1423–1437 (1994).

519 25. R. M. May, R. M. Anderson, Epidemiology and genetics in the coevolution of parasites

520   and hosts. *Proc. R. Soc. London - B. Biol. Sci.* **219**, 281–313 (1983).

521 26. M. Boots, P. J. Hudson, A. Sasaki, Large shifts in pathogen virulence relate to host

522   population structure. *Science (80-.).* **303**, 842–844 (2004).

523 27. M. Kamo, M. Boots, The evolution of parasite dispersal, transmission, and virulence in

524   spatial host populations. *Evol. Ecol. Res.* **8**, 1333–1347 (2006).

525 28. M. Kamo, A. Sasaki, M. Boots, The role of trade-off shapes in the evolution of

526   parasites in spatial host populations: An approximate analytical approach. *J. Theor.*

527   *Biol.* **244**, 588–596 (2007).

528 29. F. Mondet, J. R. de Miranda, A. Kretzschmar, Y. Le Conte, A. R. Mercer, On the front

529   line: Quantitative virus dynamics in honeybee (Apis mellifera L.) colonies along a new

530   expansion front of the parasite Varroa destructor. *PLoS Pathog.* **10**, e1004323 (2014).

531   30. C. Kelehear, G. P. Brown, R. Shine, Rapid evolution of parasite life history traits on an

532   expanding range-edge. *Ecol. Lett.* **15**, 329–337 (2012).

533   31. B. L. Phillips, R. Puschendorf, Do pathogens become more virulent as they spread?

534   Evidence from the amphibian declines in Central America. *Proc. Biol. Sci.* **280**,

535   20131290 (2013).

536   32. D. M. Hawley, E. E. Osnas, A. P. Dobson, W. M. Hochachka, D. H. Ley, Parallel

537   patterns of increased virulence in a recently emerged wildlife pathogen. *PLoS Biol.* **11**,

538   e1001570 (2013).

539   33. J. C. De Roode, A. B. Pedersen, M. D. Hunter, S. Altizer, Host plant species affects

540   virulence in monarch butterfly parasites. *J. Anim. Ecol.* **77**, 120–126 (2008).

541   34. V. Calcagno, N. Mouquet, P. Jarne, P. David, Coexistence in a metacommunity: the

542   competition-colonization trade-off is not dead. *Ecol. Lett.* **9**, 897–907 (2006).

543   35. I. Oliveri, Y. Michalakis, P.-H. Gouyon, Metapopulation Genetics and the Evolution of

544   Dispersal. *Am. Soc. Nat.* **146**, 202–228 (1995).

545   36. L. S. Nørgaard, B. L. Phillips, M. D. Hall, Infection in patchy populations: Contrasting

546   pathogen invasion success and dispersal at varying times since host colonization. *Evol.*

547   *Lett.* **3**, 555–566 (2019).

548   37. A. Kubisch, R. D. Holt, H. J. Poethke, E. A. Fronhofer, Where am I and why?

549   Synthesizing range biology and the eco-evolutionary dynamics of dispersal. *Oikos* **123**,

550   5–22 (2014).

551   38. A. M. Dunn, M. J. Hatcher, Parasites and biological invasions: Parallels, interactions,

23

552   and control. *Trends Parasitol.* **31**, 189–199 (2015).

553   39.   M. A. Brockhurst, B. Koskella, Experimental coevolution of species interactions.

554   *Trends Ecol. Evol.* **28**, 367–375 (2013).

555   40.   M. Boots, M. Mealor, Local interactions select for lower pathogen infectivity. *Science*

556   *(80-.).* **315**, 1284–1286 (2007).

557   41.   B. Kerr, C. Neuhauser, B. J. M. Bohannan, A. M. Dean, Local migration promotes

558   competitive restraint in a host-pathogen "tragedy of the commons". *Nature* **442**, 75–78

559   (2006).

560   42.   T. W. Berngruber, S. Lion, S. Gandon, Spatial structure, transmission modes and the

561   evolution of viral exploitation strategies. *PLoS Pathog.* **11**, e1004810 (2015).

562   43.   M. Boots, A. Sasaki, "Small worlds" and the evolution of virulence: infection occurs

563   locally and at a distance. *Proc. R. Soc. B-Biological Sci.* **266**, 1933–1938 (1999).

564   44.   J. Yin, Evolution of bacteriophage T7 in a growing plaque. *J. Bacteriol.* **175**, 1272–

565   1277 (1993).

566   45.   N. A. Friedenberg, Experimental evolution of dispersal in spatiotemporally variable

567   microcosms. *Ecol. Lett.* **6**, 953–959 (2003).

568   46.   B. M. Ochocki, T. E. X. Miller, Rapid evolution of dispersal ability makes biological

569   invasions faster and more variable. *Nat. Commun.* **8**, 1–8 (2017).

570   47.   E. A. Fronhofer, F. Altermatt, Eco-evolutionary feedbacks during experimental range

571   expansions. *Nat. Commun.* **6** (2015).

572   48.   S. Lion, M. Van Baalen, W. G. Wilson, The evolution of parasite manipulation of host

573   dispersal. *Proc. R. Soc. B Biol. Sci.* **273**, 1063–1071 (2006).

574   49.   H. R. Thieme, *Mathematics in population biology* (Princeton University Press, 2018).

575   50.   S. Lion, M. van Baalen, W. G. Wilson, The evolution of parasite manipulation of host

576   dispersal. *Proc. R. Soc. B-BIOLOGICAL Sci.* **273**, 1063–1071 (2006).

577   51.   E. E. Osnas, P. J. Hurtado, E. E. Osnas, Evolution of pathogen virulence across space

578   during an epidemic. *Am. Nat.* **185**, 332–342 (2015).

579   52.   G. Zilio, *et al.*, Travelling with a prasite: the evolution of resistance and dispersal

580   syndrome dyring experimental range expansion. *BioXriv* (2020)

581   https:/doi.org/http://dx.doi.org/10.1101/2020.01.29.924498.

582   53.   J. Pérez-Tris, S. Bensch, Dispersal increases local transmission of avian malarial

583   parasites. *Ecol. Lett.* **8**, 838–845 (2005).

584   54.   T. Nidelet, J. C. Koella, O. Kaltz, Effects of shortened host life span on the evolution

585   of parasite life history and virulence in a microbial host-parasite system. *BMC Evol.*

586   *Biol.* **9**, 1–10 (2009).

587   55.   H. Magalon, T. Nidelet, G. Martin, O. Kaltz, Host growth conditions influence

588   experimental evolution of life history and virulence of a parasite with vertical and

589   horizontal transmission. *Evolution (N. Y).* **64**, 2126–2138 (2010).

590   56.   O. Restif, O. Kaltz, Condition-dependent virulence in a horizontally and vertically

591   transmitted bacterial parasite. *Oikos* **114**, 148–158 (2006).

592   57.   J. Moore, *Parasites and the behaviour of animals* (Oxford University Press, 2002).

593   58.   X. Martini, M. Hoffmann, M. R. Coy, L. L. Stelinski, K. S. Pelz-Stelinski, Infection of

594   an insect vector with a bacterial plant pathogen increases its propensity for dispersal.

595   *PLoS One* **10**, 1–16 (2015).

596   59.   S. Fellous, E. Quillery, A. B. Duncan, O. Kaltz, Parasitic infection reduces dispersal of

597   ciliate host. *Biol. Lett.* **7**, 327–329 (2011).

598 60. L. S. Nørgaard, B. L. Phillips, M. D. Hall, Can pathogens optimize both transmission

599   and dispersal by exploiting sexual dimorphism in their hosts? *Biol. Lett.* **15**, 20190180

600   (2019).

601 61. C. A. Bradley, S. Altizer, Parasites hinder monarch butterfly flight: Implications for

602   disease spread in migratory hosts. *Ecol. Lett.* **8**, 290–300 (2005).

603 62. S. L. Goodacre, *et al.*, Microbial modification of host long-distance dispersal capacity.

604   *BMC Biol.* **7** (2009).

605 63. E. A. Fronhofer, F. Altermatt, Eco-evolutionary feedbacks during experimental range

606   expansions. *Nat. Commun.* **6** (2015).

607 64. D. Fels, M. Vignon, O. Kaltz, Ecological and genetic determinants of multiple

608   infection and aggregation in a microbial host-parasite system. *Parasitology* **135**, 1373–

609   1383 (2008).

610 65. A. Bauer, E. R. Haine, M. J. Perrot-Minnot, T. Rigaud, The acanthocephalan parasite

611   Polymorphus minutus alters the geotactic and clinging behaviours of two sympatric

612   amphipod hosts: The native Gammarus pulex and the invasive Gammarus roeseli. *J.*

613   *Zool.* **267**, 39–43 (2005).

614 66. S. Lion, M. Boots, Are parasites "'prudent'" in space? *Ecol. Lett.* **13**, 1245–1255

615   (2010).

616 67. O. Kaltz, J. C. Koella, L. D. P. Evolutive, U. Pierre, S. Bernard, Host growth

617   conditions regulate the plasticity of horizontal and vertical transmission in Holospora

618   undulata, a bacterial parasite of the protozoan Paramecium caudatum. *Evolution (N. Y).*

619   **57**, 1535–1542 (2003).

620 68. O. J. Burton, B. L. Phillips, J. M. J. Travis, Trade-offs and the evolution of life-

621   histories during range expansion. *Ecol. Lett.* **13**, 1210–1220 (2010).

622   69.   D. Ebert, The epidemiology and evolution of symbionts with mixed-mode

623   transmission. *Annu. Rev. Ecol. Evol. Syst.* **44**, 623–643 (2013).

624   70.   M. Su, G. Chen, Y. Yang, Dynamics of host-parasite interactions with horizontal and

625   vertical transmissions in spatially heterogeneous environment. *Phys. A Stat. Mech. its*

626   *Appl.* **517**, 452–458 (2019).

627   71.   R. Wichterman, *The biology of Paramecium* (Plenum Press, New York, 1986).

628   72.   T. Nidelet, O. Kaltz, Direct and correlated responses to selection in a host-parasite

629   system: Testing for the emergence of genotype specificity. *Evolution (N. Y).* **61**, 1803–

630   1811 (2007).

631   73.   H. D. Görtz, J. Dieckmann, Life cycle and infectivity of Holospora elegans Haffkine, a

632   micronucleus-specific symbiont of Paramecium caudatum (Ehrenberg). *Protistologia*

633   **16**, 591–603 (1980).

634   74.   S. I. Fokin, H.-D. Görtz, "Diversity of Holospora bacteria in Paramecium and their

635   characterization" in *Endosymbionts in Paramecium*, (2009), pp. 162–194.

636   75.   F. Pennekamp, N. Schtickzelle, O. L. Petchey, BEMOVI, software for extracting

637   behavior and morphology from videos, illustrated with analyses of microbes. *Ecol.*

638   *Evol.* **5**, 2584–2595 (2015).

639   76.   D. Bates, M. Machler, B. M. Bolker, S. C. Walker, Fitting linear mixed-effect models

640   using lme4. *J. Stat. Softw.* (2015).

641   77.   J. Fox, S. Weisberg, *An R companion to applied regression* (SAGE Publication Inc.,

642   2018).

643   78.   E. A. Fronhofer, *et al.*, Bottom-up and top-down control of dispersal across major

644   organismal groups: a coordinated distributed experiment. *Nat. Ecol. Evol.*, 213256

645   (2017).

646

647

648 **Fig. 1.** Experimental design of the long-term selection experiment, using 2-patch dispersal

649 systems. Infected populations were placed in the 'core' tube and allowed to disperse to the other

650 'front' tube during 3 h (horizontal arrows). In the front selection treatment (red), only the

651 dispersing fraction of the population was maintained, whereas in the core selection treatment

652 (blue) only the non-dispersing fraction was maintained. After adjustment of initial densities,

653 the selected fractions were then transferred to a new tube (vertical arrows) and grown for 1

654 week, during which time demographic and epidemiological processes acted freely. A total of

655 55 dispersal/growth cycles were performed, for 5 core and 5 front selection lines.

656

657 **Fig. 2.** Dispersal and infection life-cycle traits of evolved parasites from core selection (blue)

658 and front selection (red) treatments, measured on naïve *Paramecium*. **(A) Dispersal rate**.

659 Proportion of dispersing infected hosts observed in infected assay cultures placed for 3 h in a

660 dispersal system. **(B) Infectivity.** Proportion of infected hosts in assay cultures on day 4 post-

661 inoculation (p.i.). **(C) Infectiousness**. Proportion of infectious hosts in infected assay cultures

662 between day 6 and 11 p.i.. Infectious hosts are individuals that produce infective spores of the

663 parasite. **(D) Virulence.** Association between infected host division and survival, expressed

664 relative to uninfected hosts (infected minus uninfected). Negative values indicate negative

665 effects of infection on the host trait. Panels (A)-(C) show means and 95 % confidence intervals

666 of the model predictions. Small insert panels show predictive distributions (and 95% CI) of the

667 difference between front and core treatments. Symbols represent observed means for different

668 combinations of parasite selection line and assay host genotype. Different symbols refer to
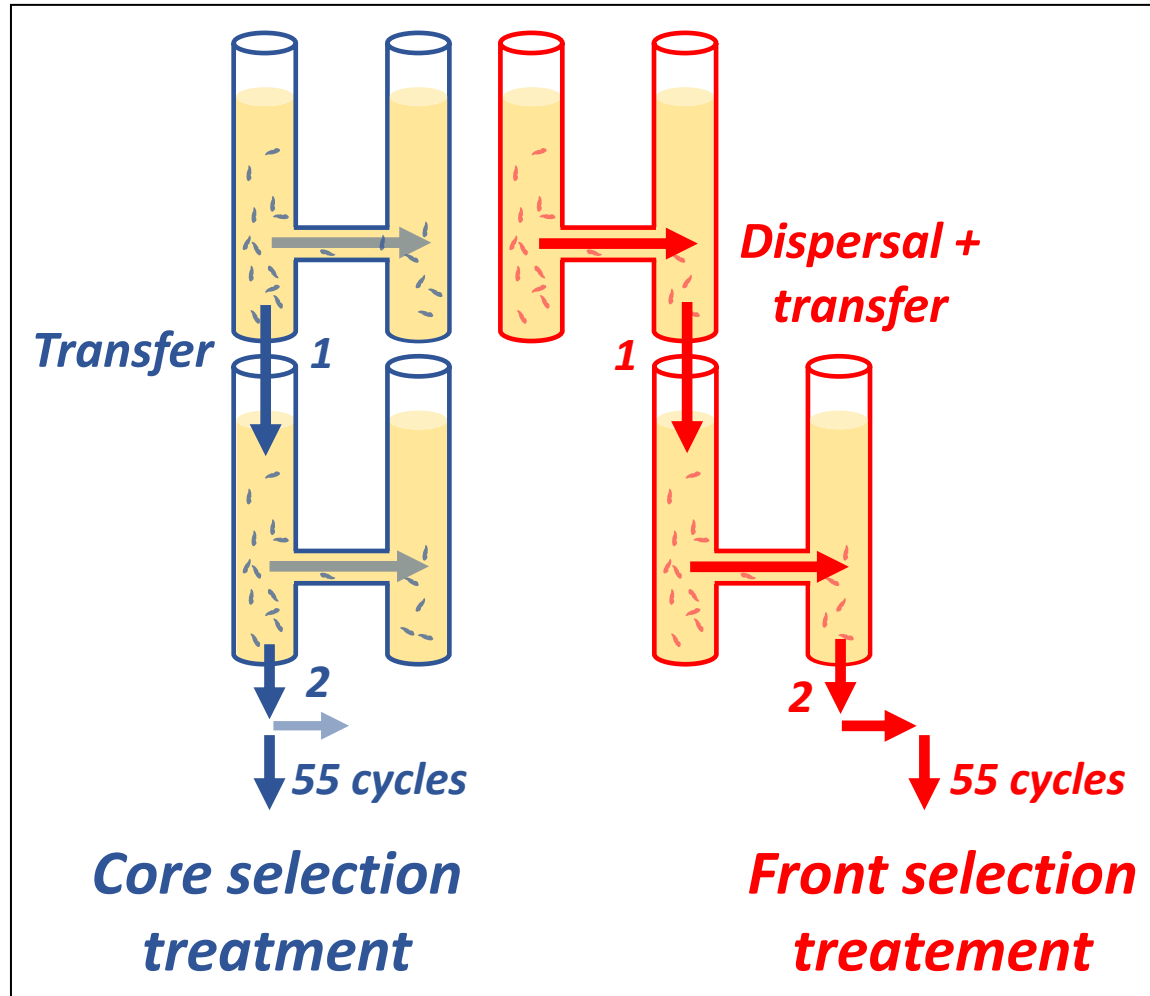
669 different parasite selection lines (n = 10).

670

29

671 **Fig. 3.** Estimates of virulence of evolved parasites from core selection (blue) and front selection

672 (red) treatments, measured on naïve *Paramecium*. **(A) Host division**. Maximum cell density of

673 infected and uninfected *Paramecium*, as determined in a singleton assay. **(B) Host survival.**

674 Proportion of surviving infected and uninfected replicates on day 20 in the singleton assay. All

675 panels show means and 95 % confidence (CI) intervals of the model predictions. Small insert

676 panels show predictive distributions (and 95% CI) of the difference between front and core

677 treatments. Symbols represent observed means for different combinations of parasite selection

678 line and assay host genotype. Different symbols refer to different parasite selection lines (n =

679 10).

680

681 **Fig. 4.** Relationships between parasite traits. **(a)** Path analysis testing direct and indirect effects

682 of 4 parasite traits on infected host dispersal: (i) Infectiousness (cumulative proportion of host

683 producing infective spores; area under the curve: day 6 - 11 p.i.); (ii) Host division (maximum

684 infected cell density); (iii) Swimming tortuosity ($\approx$ trajectory changes) and (iv) net swimming

685 speed of infected singletons. Analysis based on trait means for different combinations of

686 parasite selection line and host assay genotype (n = 25) and performed on residuals, after

687 correcting for overall effects of host assay genotype. Standardised beta regression coefficients

688 (β) are shown above arrows ($*p < 0.05$); **(b)** Relationship between residual host division and

689 dispersal; **(c)** Relationship between residual horizontal transmission investment and host
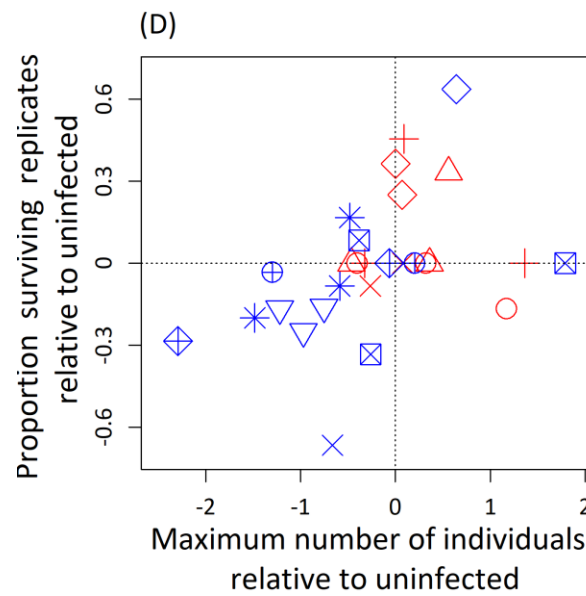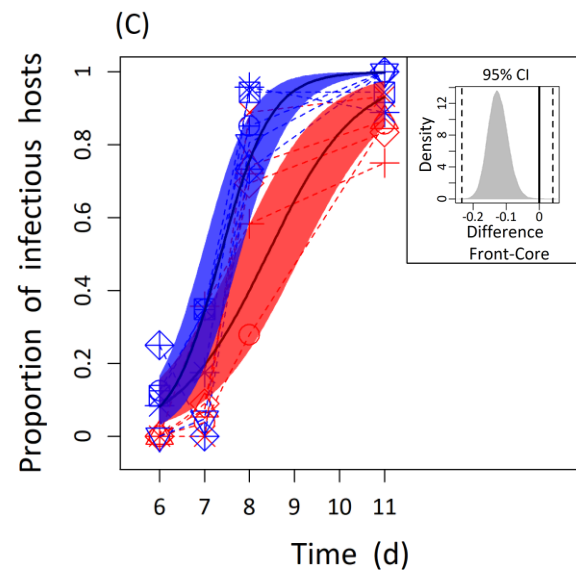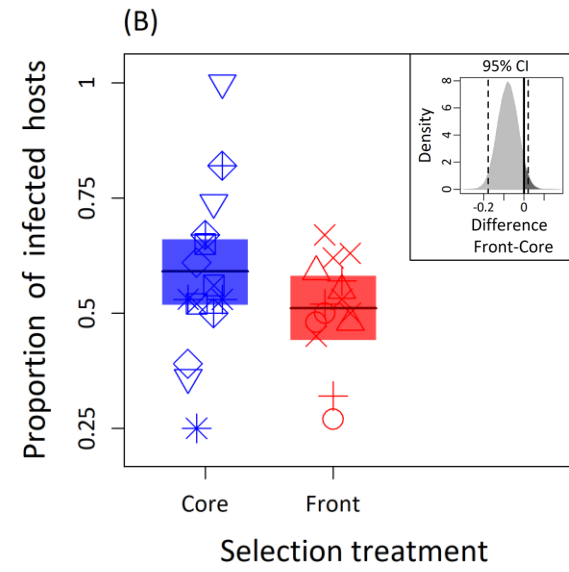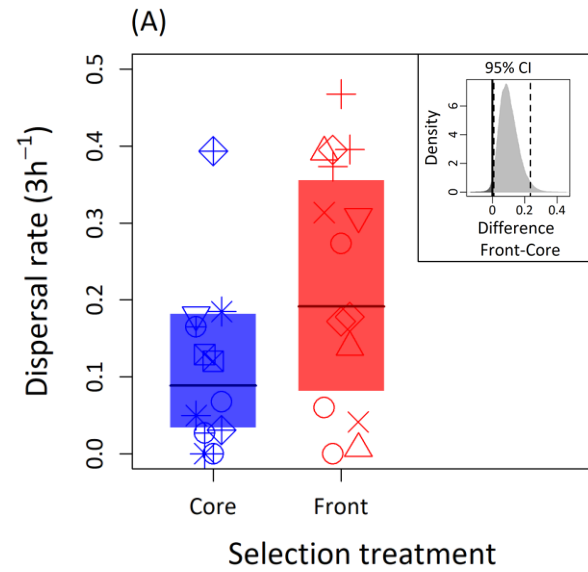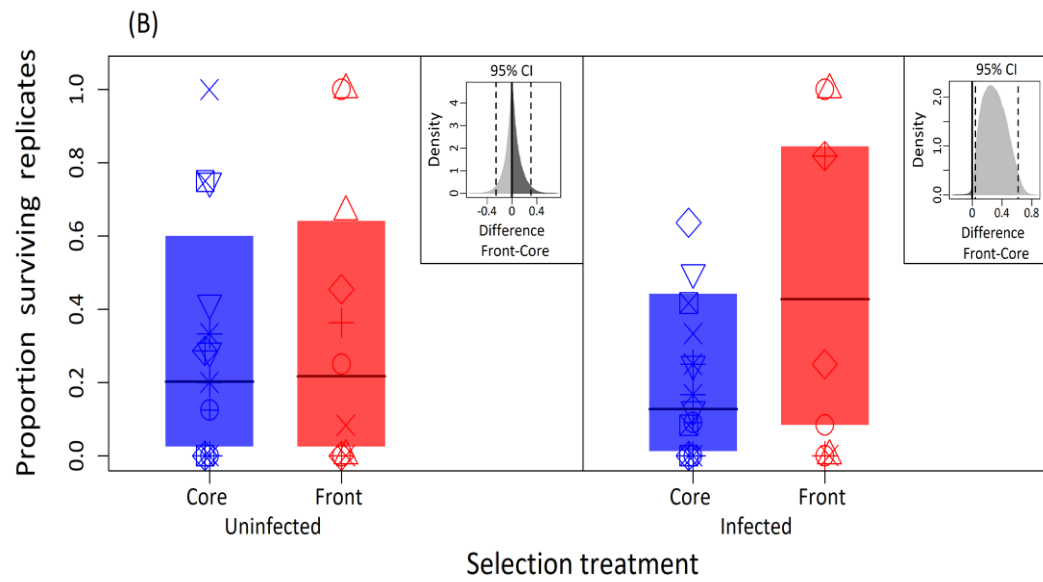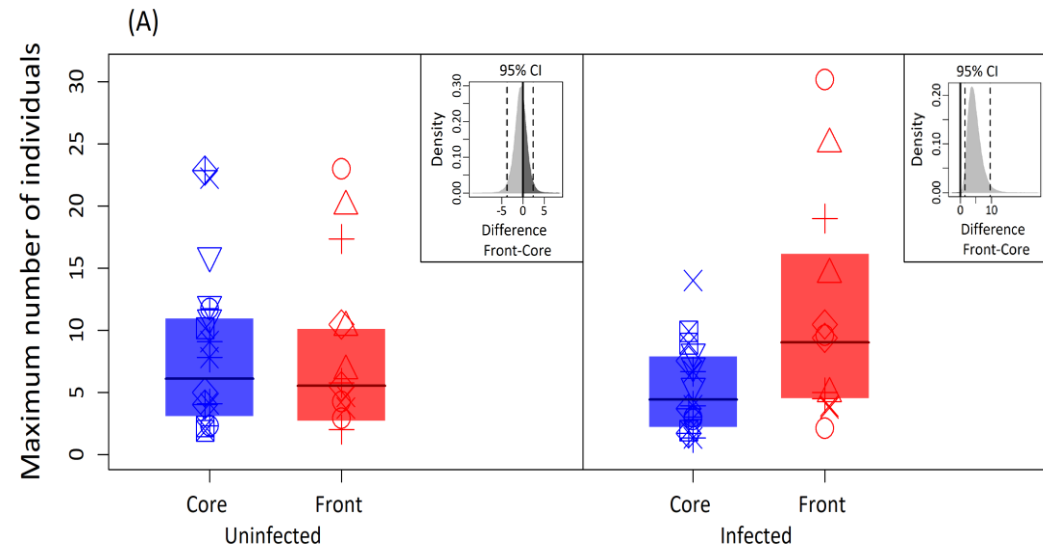
690 division.

691

692 **Fig. 5.** Fit of the epidemiological model. **(a)** Fit of the epidemiological model (equations 6-8)

693 to infected and uninfected host density time-series data, obtained for assay cultures infected

694 with core (blue) and front (red) parasites. Curve fits shown for host genotype 63D (for other

30

695   genotypes, see Fig. S11). Dashed lines represent observed densities for different replicate assay

696   cultures, solid lines and shaded areas represent posterior model predictions (mean and 95% CI).

697   **(b)-(d)** Posterior distributions for virulence (= reduction in host division rate), horizontal

698   transmission rate and latency, respectively. Solid lines and shaded areas show posterior

699   distributions for host genotype 63D, dashed lines for host genotype C173, and the dotted lines
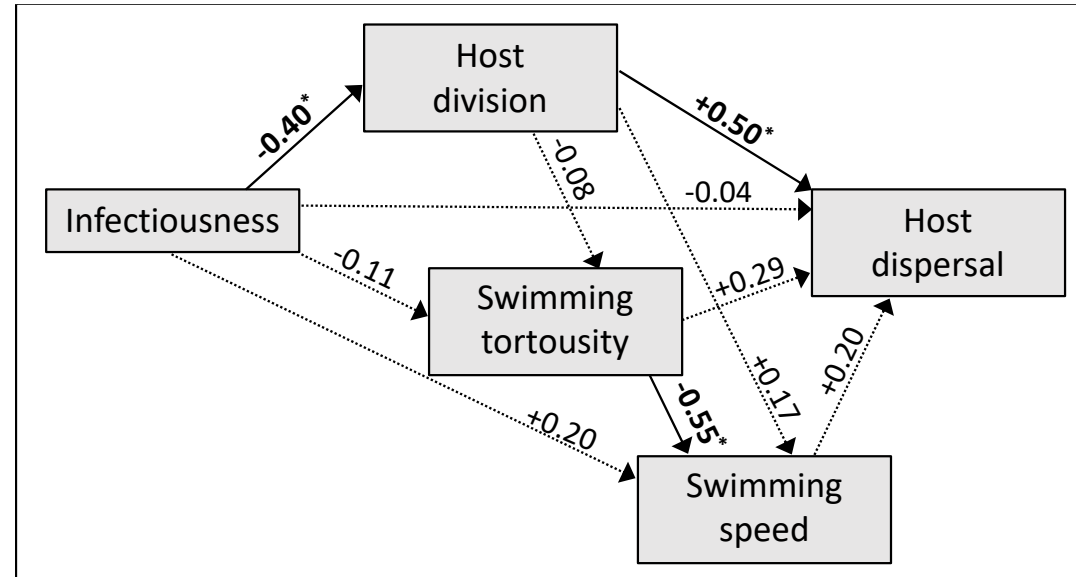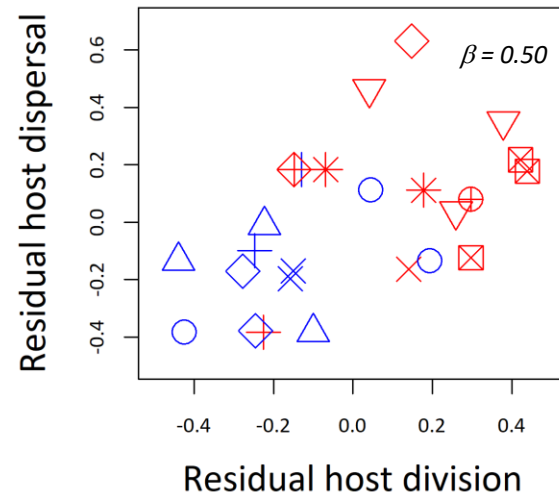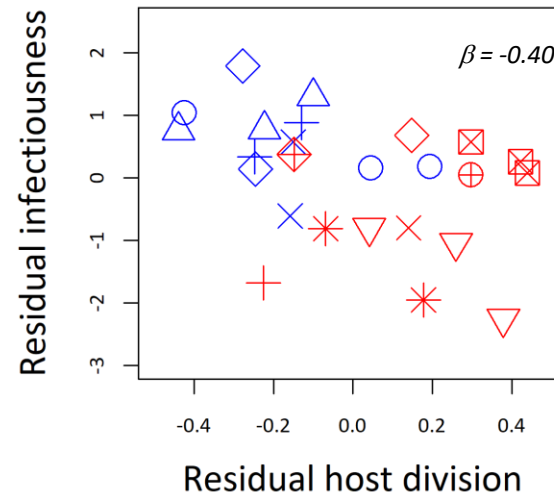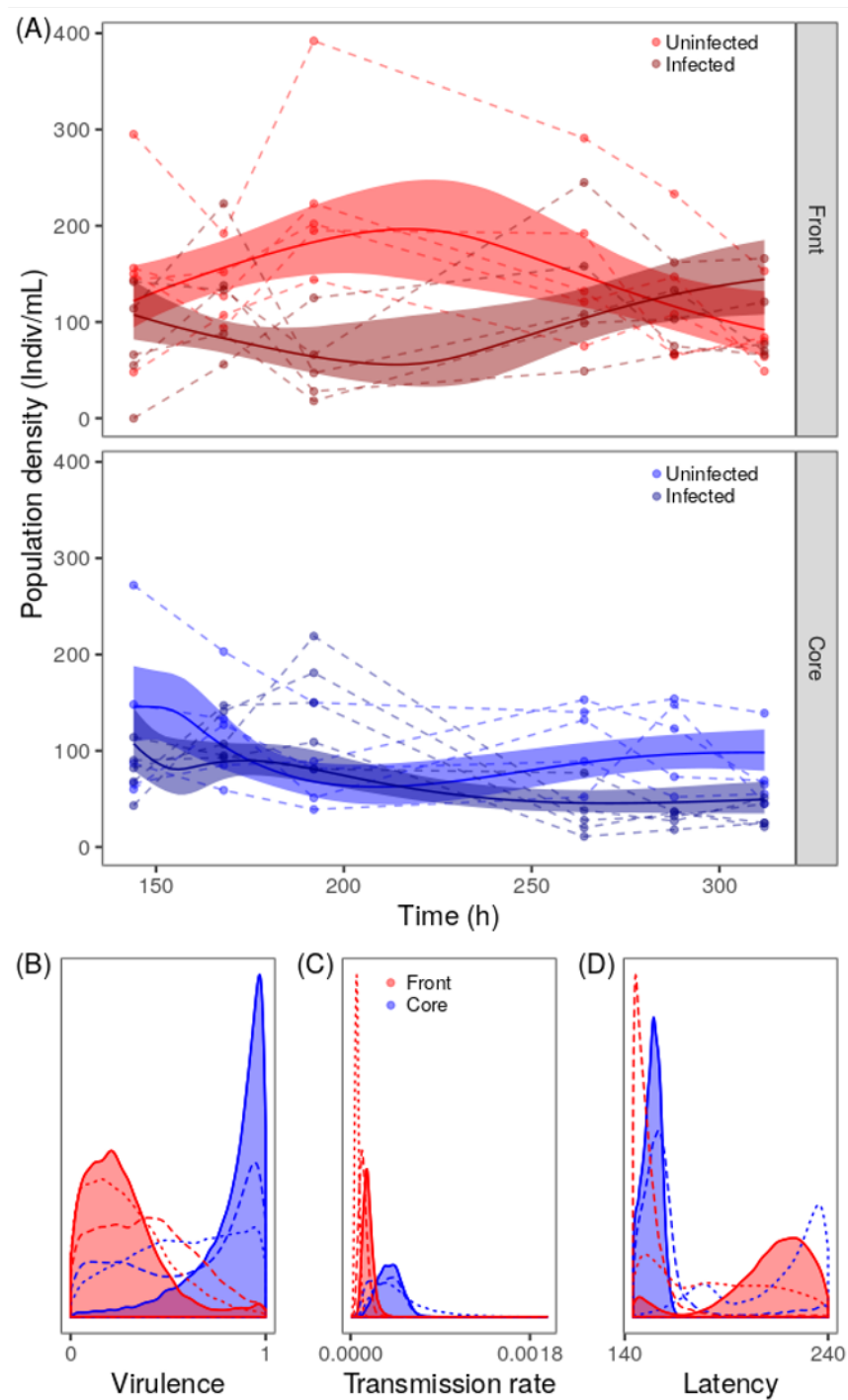
700   for genotype C023.

Transfer

Dispersal + transfer

1

1

2

2

55 cycles

55 cycles

Core selection treatment

Front selection treatement

(A)

(B)

(A)

Host division

Infectiousness

Swimming tortousity

Host dispersal

Swimming speed

-0.40*   **+0.50***   -0.08   -0.04   -0.11   +0.29   **-0.55***   +0.17   +0.20   +0.20

(B)

$\beta = 0.50$

Residual host dispersal

Residual host division

(C)

$\beta = -0.40$

Residual infectiousness

Residual host division

Supplementary Information

5 # An evolutionary trade-off between parasite virulence and dispersal at experimental invasion fronts

Louise Solveig Nørgaard[1,2#*], Giacomo Zilio[2#], Camille Saade[2],
Claire Gougat-Barbera[2], Matthew D. Hall[1], Emanuel A. Fronhofer[2] & Oliver Kaltz[2*]

10   [1]School of Biological Sciences and Centre for Geometric Biology, Monash University, Melbourne 3800, Australia
[2]ISEM, University of Montpellier, CNRS, EPHE, IRD, Montpellier, France.

SI 1: Long-term selection protocol

Dispersal arenas consisted of two 14 mL plastic tubes (the core and front patch, Fig. S1) interconnected by a 5 cm silicon tube of 0.6 mm inner diameter (corridor). The protocol for a dispersal event is as follows. Step 1: We first fill the entire arena with 9.5 mL of fresh growth medium, then block the corridor with a clamp. Step 2: one of the two tubes ("core patch") is topped up to 13 mL with 8 mL of medium containing cultures of *Paramecium caudatum* *('Paramecium', hereafter)*, while the other tube ("front patch") is topped up to 13 mL with medium only. Step 3: we remove the clamp for 3 h allowing the *Paramecium* to actively disperse from core to front patch or to stay in the core patch. Step 4: after blocking the corridor again, population densities in core and front patches are determined from 200-µL samples, with the number of individuals counted under a dissecting microscope. From these counts we can estimate the dispersal rate.
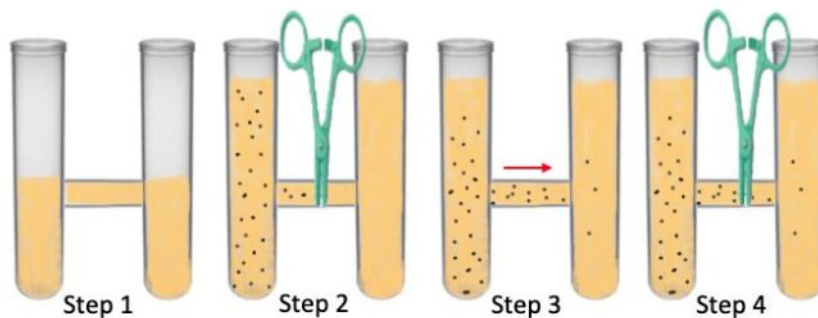
Figure S1. Protocol for setting up dispersal events in 2-patch dispersal arena. Step 1: filling dispersal arean up until dispersal corridor with fresh growth medium. Step 2: block corridor with a clamp and add cultures of *Paramecium* to patch 1 and fresh media to patch 2. Step 3: remove clamp and allow for acrive dispersal from patch 1 to patch 2 during a three-hour period. Step 4: block dispersal corridor and assess population densities and infection status in patch 1 and 2.

Using a mix of parasite inocula we infected naïve *Paramecium* of the 63D genotype to set up five front selection and five core selection lines (see main text for details on host and parasite origins). The long-term selection protocol is as follows (for illustration, see Fig. 1 in main text).

(i) In the front selection treatment, densities in the core patch prior to dispersal were set to c. 2000 individuals. After the 3 h of free dispersal, only *Paramecium* that dispersed to the front patch were maintained, transferred to a 50-mL plastic tube and cultured for one week in 20 mL of bacterised lettuce medium, before the next dispersal and selection event occurred. On average, c. 350 individuals dispersed at a given dispersal event. When we observed fewer than 100 dispersers, we topped up numbers to 100 by adding non-dispersers. Over the one week of culture, populations grew back to carrying capacity (c. $4\text{-}5 \times 10^3$ individuals) and epidemiological processes were acting freely. Then a new episode of dispersal occurred, as described above.

(ii) In the core selection treatment, we followed the same protocol as above, but only *Paramecium* that stayed in the core patch were maintained and regrown in 20 mL of medium. Furthermore, numbers of transferred core individuals were adjusted so as to match those in the front selection treatment at the beginning of the one-week growth period.

After 30 dispersal/growth cycles, we extracted infectious forms from each selection line and used them to inoculate a new batch of 63D hosts. This was done to minimise effects of host evolution in the experiment and to continue parasite evolution on naïve hosts for another round of 25 cycles. Because carrying capacity in this new round (c. $3\text{-}4 \times 10^3$ individuals) was lower

2

55 than in the first 30 cycles, we relaxed the dispersal protocol. Instead of adjusting the density prior to dispersal, we topped up the core patch with the maximum possible volume (8 mL; step 2, see above) to ensure that at least 10^3 were placed in the tube.

SI 2: Assay details

60 After inoculation of three naive host genotypes (63D, C023, C173) with evolved core and front parasites, a series of assays were performed over a 3-week period. In this section, we present an overview of the timing of the assays (Table S1) and further details on the experimental protocols.

Table S1. Timing of measurements for the different parasite traits in the assay. The assay was started by
65 inoculating naive cultures of three host genotypes with parasites from 5 core and 5 front selection treatments (30 combinations in total). Timing of each assay is expressed in days post inoculation (p.i.). On day 4 p.i., the initial 30 inoculated replicates were split into three technical assay replicates, giving a total of 90 assay replicates. For certain traits, not all replicate cultures were available, or data are missing. The 'Number' columns indicate the number of combinations and replicate assay cultures available for each analysis. 'Total n' refers to the total number
70 of data points in the analysis (raw data). *Paramecium* for the singleton assay were isolated from the initial 30 inoculated assay cultures. For details on trait measurements, see SI below and main text.

| Trait	Assay day (p.i.)	Number of host x parasite combinations (max. 30)	Number of assay replicate cultures (out of total)	Total n (raw data)	Comments
Infectivity	4	30	30/30	30	
Infectiousness	4 - 11	30	90/90	147	First infectious hosts detected on day 6 p.i.
Infected dispersal	13 - 19	27	75/90	75	Exclude replicate cultures if low density / infection prevalence (<10%)
Virulence (Host division and survival in singleton assay)	13 - 23	28	28/30	605	Infected and uninfected individuals isolated on day 4 p.i. and grown for 9 days under common-garden conditions prior to singleton assay
Movement (tortuosity and swimming speed)	14	29	29/30	106	Video analysis performed on infected and uninfected populations isolated on day 4 p.i.

Infectivity

75 **Inoculum preparation.** To extract infectious forms of *Holospora undulata* from an infected culture, the infected *Paramecium* are transferred to 50-mL Falcon tubes and centrifuged at 1500 g for 20 minutes. The supernatant is removed, and the concentrated individuals placed in 1.5 mL Eppendorf tubes containing 1 mm glass beads. Using a Qiagen TissueLyser they are then vortexed and crushed (1:45 minutes at 30 oscillation frequency) to liberate infectious forms of
80 the parasite. The concentration of infectious forms is then determined at 200x magnification under a microscope (Leica DM LB2), using a hemocytometer.

Infectivity assay. Inocula of the evolved parasites selected for high or low dispersal (see Fig. S2; front and core, respectively) were prepared, as described above. Their capacity to establish infections (= infectivity) was tested on samples of unselected naïve hosts, represented by three genotypes: 63D, C023 and C173. Prior to inoculation, cultures of the three genotypes were concentrated by using mild centrifugation (15 min at 300 g). We placed ≈ 5 x 10^3 cells of a given host genotype in 1.4 mL of bacterised medium in a 15 mL tube, to which we added the freshly prepared inoculum of a given evolved parasite line. Inoculum dose ranged from c. 0.3 - 1.4 x 10^3 infective spores per μL (median: 1 x 10^3), depending on the identity of parasite selection line. These doses represent an *ad libitum* administration; typically, infection success reaches a plateau for doses > 0.2 spores per μL (Fels et al 2008). In the present experiment, a preliminary logistic regression with binomial error structure (logit link) revealed no significant effect of spore dose on infection success ($\chi_1^2 = 10.812$, p = 0.147).

Dispersal assay

In the assay, we used 3-patch arenas (50-mL Falcon tubes; Fig. S3) instead of the usual 2-patch arena. These arenas allowed us to use larger numbers of *Paramecium* and, by letting them disperse from the middle tube into the two outer tubes, we increased the total number of dispersers. To further increase the resolution of dispersal estimates, we concentrated the cultures 12 h prior to the assay, by gentle centrifugation at 300 g for 15 minutes. For the dispersal assay, we first filled the 3-patch system with 20 mL of fresh medium, and then blocked the two corridors with clamps (see steps 1 and 2 in Fig. S1). We then added ≈2800 individuals to the middle tube and topped it up to 25 mL with fresh medium. The outer tubes were topped up to 25 mL with fresh medium only, and the corridors were then opened for 3 h to allow for free dispersal. At the end of the 3-h dispersal period, we determined population density and infection prevalence, for samples from the central tube (500 μl) and from the combined two outer tubes (3 mL). From these estimates we calculated the dispersal rate of infected hosts, as explained above. Of the 90 inoculated replicate assay cultures, 88 were tested (two tubes were found to be uninfected). For statistical analysis, we excluded 13 replicates with very low population density and/or low infection prevalence (<10%), which prevented accurate estimation of dispersal of infected individuals. We also assayed a small number of uninfected control cultures (three tubes per host genotype) for comparison with dispersal rates in infected tubes. For unknown reasons, these replicates showed considerable variation; we therefore regrouped these observations with measurements from previous experiments to inform on the general range of dispersal rates observed for these genotypes (see Fig. S4). We did not carry out formal statistical comparisons with infected dispersal rates observed in our assay.
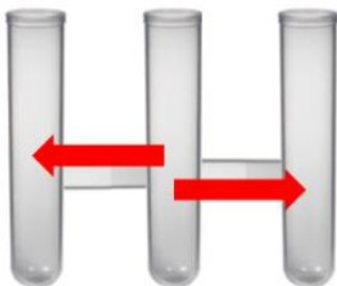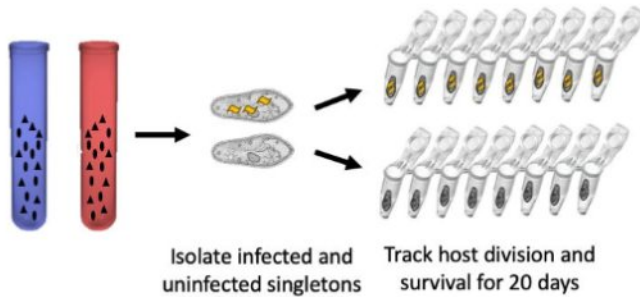

Figure S2. Linear 3-patch arenas used for the dispersal assays. *Paramecium* was added in the central tube and after the opening of the connections it was allowed to disperse (3h) in the outer tubes, as indicated by the red arrows. For filling protocol, see Fig. S1.

Virulence assay

For the virulence assay, we isolated single infected and uninfected individuals from the replicate assay cultures on day 4 p.i and allowed them to multiply in 2-mL Eppendorf tubes with bacterised medium, under permissive common-garden conditions. After one week, we

4

135   determined infection status of these monoclonal cultures (LAO fixation). On day 13 p.i., we started the assay by placing single individuals in PCR tubes filled with 200 μL of bacterised medium (Fig. S3). We checked tubes daily for presence or absence of live cells for 20 days. In addition, cell density was determined on day 2 and 3 (by counting cells through the plastic tubes), on day 10 (from 50-μL samples) and on day 20 (total volume). Except for 50 μL of medium added on day 10, no resources were supplied.

Isolate infected and uninfected singletons

Track host division and survival for 20 days

Figure S3. Protocol for virulence assay. On day 4 post inoculation of replicate cultures with front (ref) or core (blue) parasites, infected and uninfected individuals were isolated and allowed to grow as small monoclonal cultures. Single individuals were then placed PCR tubes containing 200 μL bacterised medium. Each combination of parasite selection line (n = 10) and host genotype (n = 3) was replicated 8-12 times.

155   The assay was performed for 28 of the 30 combinations of parasite selection line and host genotypes, with 8-12 infected singletons tested per combination. Of the 322 infected replicates, 17 died within less than 24 h (possibly due to transfer handling) and were excluded from statistical analysis. In the same way, excluded 23 early deaths of the 323 uninfected singletons.

SI 3: Results

160 The assays of the evolved parasites were performed on naïve *Paramecium* representing three host genotypes (63D, C172, C023). The parasites had evolved on the 63D genotype in the selection experiment, but had never been exposed to any of the other two genotypes. In our main statistical analyses, we considered host genotype as a random effect, as the experimental tests were not specifically meant to address differences among the host genotypes. These results

165 are summarised in Table S2.

Table S2. ANOVA results from GLMM models of all measured traits (dispersal, swimming speed and tortuosity, infectivity, infectiousness and virulence). Parasite selection line and host genotype were added as random factors, all other factors were considered fixed. We performed

170 backward model simplification, with sequential removal on non-significant terms in the model. Terms in the "Fixed effects" category represent the minimal adequate model; sequentially removed terms appear in the "Eliminated terms" category. For each analysis, we indicate the number of replicates used in the analysis and the number of host genotype x parasite selection lines they represent (3 x 10 = 30 combinations inoculated, some of which were not available for

175 certain analyses).

(a) Dispersal

Random effect:	Var		
Selection line	0.43		
Host genotype	0.39		
Fixed effects:	*d.f.*	χ^2	p
Selection treatment	1	4.9	0.027 *

N = 75, data from 28/30 host genotype x selection line combinations

(b) Swimming speed

Random effect:	Var		
Selection line	<0.001		
Host genotype	<0.001		
Eliminated terms:			
Selection treatment	1	0.67	0.414
Infection status	1	1.25	0.262
Treatment x infection status	1	0.33	0.943

N = 106, data from 29/30 host genotype x selection line combinations

(c) Tortuosity

Random effects	Var		
Selection line	<0.001		
Host genotype	<0.001		
Eliminated terms:			
Selection treatment	1	0.03	0.857
Infection status	1	<0.01	0.981
Treatment x infection status	1	0.11	0.737

N = 106, data from 29/30 host genotype x selection line combinations

(d) Infectivity

Random effects	Var		
Selection line	0.03		
Host genotype	0		
Fixed effects:	*d.f.*	χ^2	p
Selection treatment	1	2.43	0.118

N = 30, data from 30/30 host genotype x selection line combinations

6

Table S2 (cont.)

(e) Infectiousness

Random effect:	Var			
Selection line	0.11			
Host genotype	0.32			
Fixed effects:	*d.f.*	χ^2	p	
Selection treatment	1	13.2	<0.001	***
Time	1	178.1	<0.001	***
Treatment x time	1	13.5	<0.001	***

N = 88, data from 30/30 host genotype x selection line combinations

(f) Maximum host density

Random effect:	Var			
Selection line	0.10			
Host genotype	2.50			
Fixed effects:	*d.f.*	χ^2	p	
Infection status	1	1.7	0.194	
Selection treatment	1	4.9	0.027	*
Treatment x Infection status	1	16.9	<0.001	***

N = 605, data from 28/30 host genotype x selection line combinations

(g) Host survival

Random effect:	Var			
Selection line	1.07			
Host genotype	2.50			
Fixed effects:	*d.f.*	χ^2	p	
Infection status	1	<0.1	0.987	
Selection treatment	1	3.4	0.065	
Treatment x Infection status	1	7.4	0.006	**

N = 605, data from 28/30 host genotype x selection line combinations

180   To inspect the generality of selection treatment effects, we also performed analyses, treating host genotype as a fixed effect and including the selection treatment x host genotype interaction (Table S3). They are accompanied by a more detailed presentation of trait expression, with separate panels for each host genotype (Fig. S4-S10). These additional analyses showed that, with few exceptions, differences between core and front parasites were consistent across the

185   different hosts (i.e., treatment x host interactions were non-significant), even though in some cases more or less pronounced. For details of trait definitions and measurements, see main text.

Table S3. ANOVA results from GLMM models of all measured traits (dispersal, swimming speed and tortuosity, infectivity, infectiousness and virulence). Parasite selection line was treated

190   as a random effect, all other factors were fixed effects. We performed backward model simplification, with non-significant terms sequentially removed from the model ("eliminated terms"). For each analysis, we indicate the number of replicates and the number of host genotype x parasite selection lines they represent (3 x 10 = 30 combinations inoculated, some of which were not available for certain analyses).

(a) Dispersal

Random effect:	Var			
Selection line	0.41			
Fixed effects:	d.f.	χ^2	p	
Selection treatment	1	7.0	0.007	**
Host genotype	2	607.5	<0.001	***
Treatment x genotype	2	22.8	<0.001	***

N = 75, data from 27/30 host genotype x selection line combinations

(b) Swimming speed

Random effect:	Var			
Selection line	2866			
Fixed effects:	d.f.	χ^2	p	
Selection treatment	1	0.6	0.404	
Host genotype	2	0.05	0.974	
Treatment x genotype	2	10.2	0.006	**
Eliminated terms:				
Infection status	1	1.1	0.286	
Infection status x genotype	1	<0.1	0.979	
Treatment x infection status	1	0.9	0.319	
Treatment x infection status x genotype	2	0.7	0.684	

N = 106, data from 29/30 host genotype x selection line combinations

(c) Tortuosity

Random effects:	Var		
Selection line	<0.01		
Fixed effects:	d.f.	χ^2	p
Selection treatment	1	0.6	0.800
Host genotype	2	1.0	0.598
Infection status	2	<0.1	0.932
Treatment x genotype	2	4.6	0.095
Infection status x genotype	2	3.7	0.157
Treatment x infection status	1	0.1	0.713
Treatment x infection status x genotype	2	3.8	0.147

N = 106, data from 29/30 host genotype x selection line combinations

(d) Infectivity

Random effects:	Var		
Selection line	0.03		
Table S3 (cont.)			
Fixed effects:	d.f.	χ^2	p
Selection treatment	1	2.44	0.118

| Host genotype | 2 | 0.01 | 0.991 | |
| Treatment x genotype | 2 | 4.33 | 0.114 | |

N = 30, data from 30/30 host genotype x selection line combinations

(e) Infectiousness

Random effect:	Var			
Selection line	0.08			
Fixed effects:	*d.f.*	χ^2	p	
Selection treatment	1	13.6	<0.001	***
Time	1	176.1	<0.001	***
Host genotype	2	28.9	<0.001	***
Treatment x time	1	16.8	<0.001	***
Treatment x host	2	10.1	0.006	**
Eliminated terms:				
Host x time	2	3.5	0.167	
Treatment x host x time	2	2.2	0.317	

N = 88, data from 30/30 host genotype x selection line combinations

(f) Maximum host density

Random effect:	Var			
Selection line	0.09			
Fixed effects:	*d.f.*	χ^2	p	
Infection status	1	2.03	0.153	
Selection treatment	1	5.4	0.019	*
Host genotype	2	264.9	<0.001	***
Treatment x Infection status	1	19.1	<0.001	***
Treatment x host	2	61.7	<0.001	***
Eliminated terms:				
Infection status x Host	2	2.7	0.258	
Treatment x Infection status x Host	2	1.5	0.457	

*N = 605, data from 28/30 host genotype x selection line combinations*

(g) Host survival

Random effect:	Var			
Selection line	0.98			
Fixed effects:	*d.f.*	χ^2	p	
Infection status	1	0.01	0.911	
Selection treatment	1	4.0	0.043	*
Host genotype	2	75.0	<0.001	***
Treatment x Infection status	2	8.2	0.004	**
Treatment x Host	1	25.9	<0.001	***
Eliminated terms:				
Infection status x Host	2	0.2	0.882	
Treatment x Infection status x Host	2	1.8	0.398	

*N = 605, data from 28/30 host genotype x selection line combinations*

195

Dispersal

200
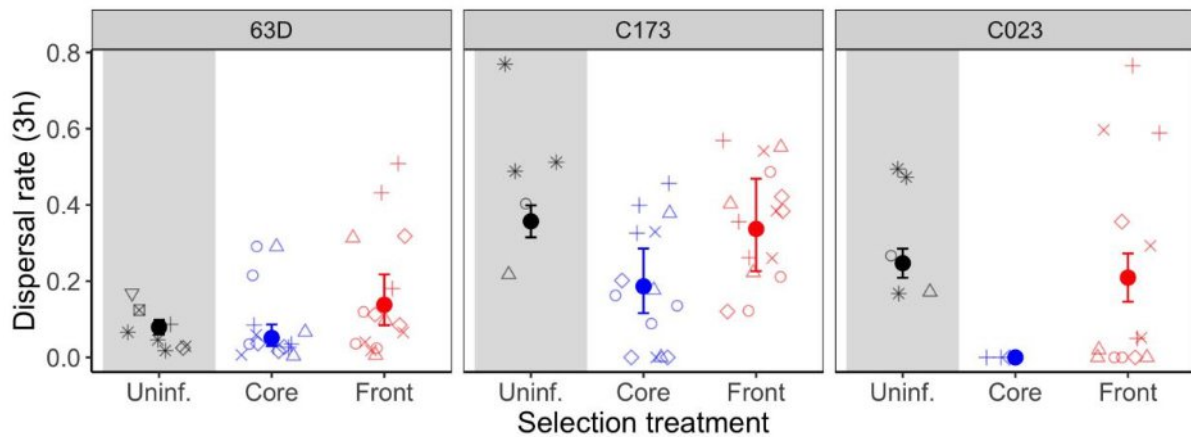
Figure S4. Dispersal rate (3 hr) of three naïve *Paramecium* genotypes (63D, C173, C023), infected with core parasites (blue) or front parasites (red). Data of uninfected replicates (black) from this assay and other experiments indicate the typical range of dispersal for each genotype (low for 63D, higher for C173 and C023). Filled circles and error bars represent means ± 95% confidence interval. Open symbols represent raw data. Different symbols refer to different parasite selection lines (5 lines per selection treatment).

Net swimming speed
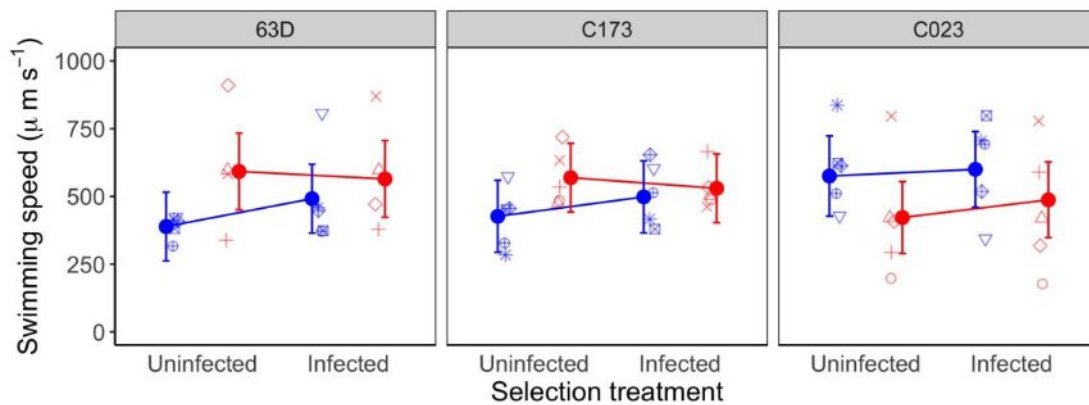
210 **Figure S5**. Net swimming speed (μm s^{-1}) of three naïve *Paramecium* genotypes (63D, C173, C023), when uninfected or infected with core parasites (blue) or front parasites (red). Filled circles and error bars represent mean model predictions ± 95% confidence interval. Open symbols represent means over two technical replicates. Different symbols refer to different parasite selection lines (5 lines per selection treatment).

215

Tortuosity - trajectory variation
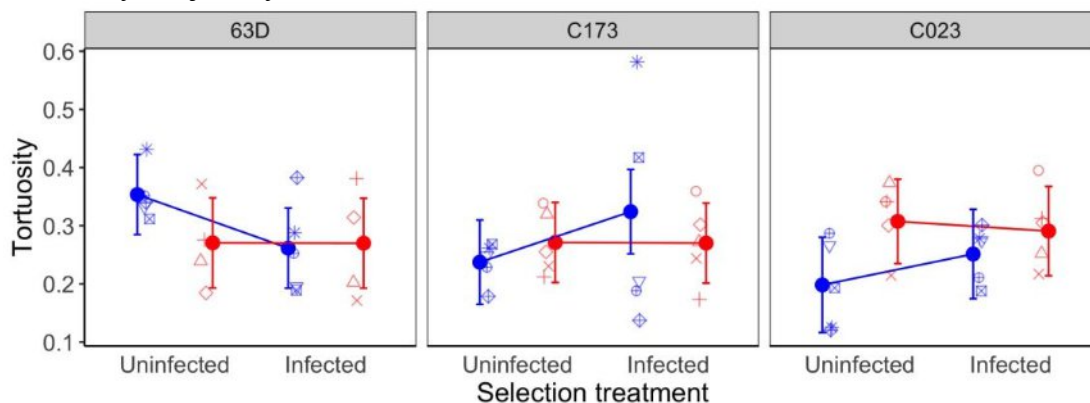
10

Figure S6. Swimming trajectory changes (tortuosity = standard deviation of turning angle distribution) of three naïve *Paramecium* genotypes (63D, C173, C023), when uninfected or infected with core parasites (blue) or front parasites (red). Filled circles and error bars represent mean model predictions ± 95% confidence interval. Open symbols represent means over two technical replicates. Different symbols refer to different parasite selection lines (5 lines per selection treatment).

Infectivity
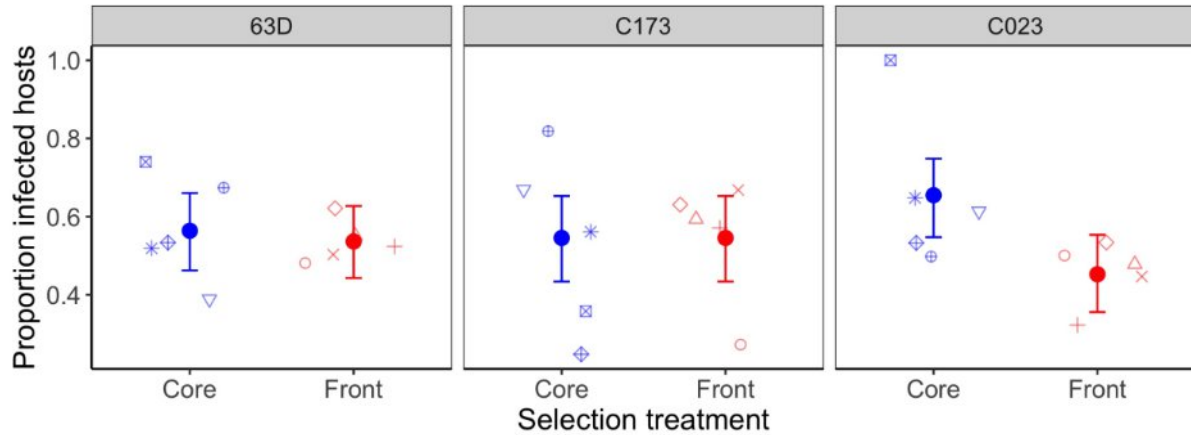
Figure S7. Proportion of infected individuals in assay cultures of three naïve *Paramecium* genotypes (63D, C173, C023), measured on day 4 post inoculation with core parasites (blue) or front parasites (red). Filled circles and error bars represent mean model predictions ± 95% confidence interval. Open symbols represent raw data. Different symbols refer to different parasite selection lines (5 lines per selection treatment). Note that these data were obtained before to splitting each culture into the 3 technical replicates (see Material and Methods in main text).
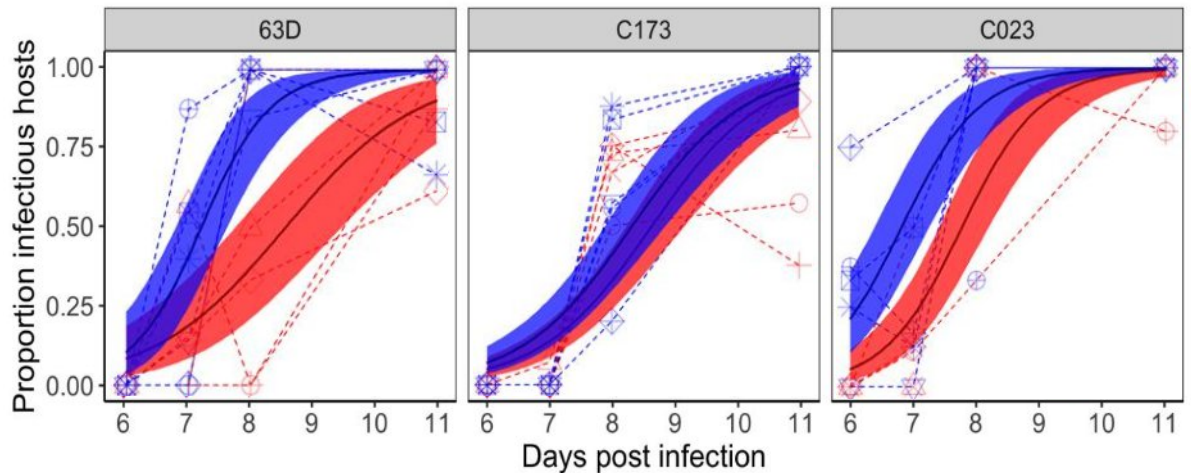
Infectiousness

Figure S8. Infectiousness (proportion of infectious hosts, i.e., individuals host carrying infective spores) on day 6, 7, 8 and 11 post inoculation (p.i.), shown for three naïve *Paramecium* genotypes (63D, C173, C023) infected with core parasites (blue) or front parasites (red). Filled circles and error bars represent mean model predictions ± 95% confidence interval. Solid lines represent mean trajectories, stippled lines represent raw data trajectories for different parasite selection lines (note that certain trajectories are superimposed). Day 6 p.i. was the first day of detection of infectious hosts.
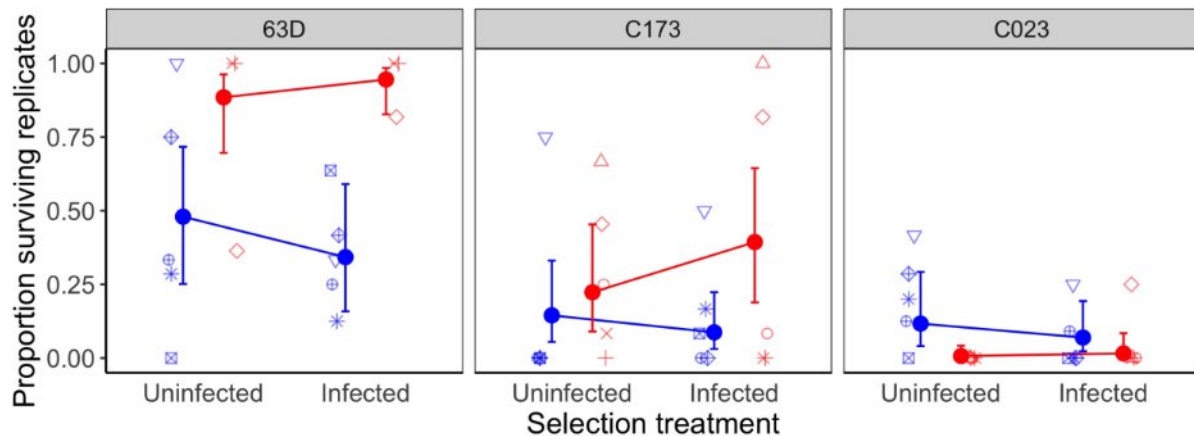
11

Virulence (I): Host division
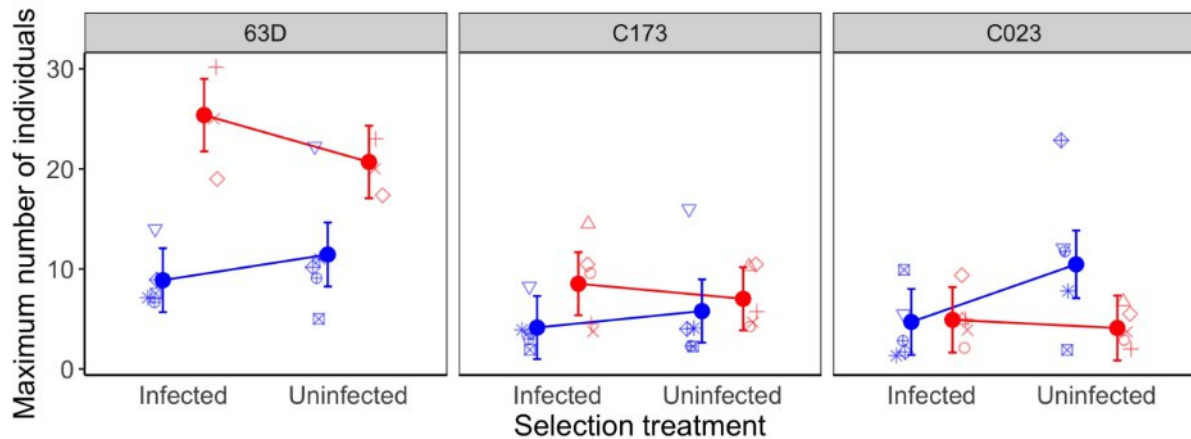
Figure S9. Maximum cell density of three naïve *Paramecium* genotypes (63D, C173, C023), when uninfected or infected with core parasites (blue) or front parasites (red). Data obtained in a 20-day assay, starting from single individuals, where maximum densities were generally reached on day 10, although some samples died sooner and thus peaked earlier. Filled circles and error bars represent mean model predictions ± 95% confidence interval. Open symbols represent means over c. 10 technical replicates, on average. Different symbols refer to different parasite selection lines (5 lines per selection treatment).

Virulence (II): Host survival

Figure S10. Mortality of three naïve *Paramecium* genotypes (63D, C173, C023), when uninfected or infected with core parasites (blue) or front parasites (red). Data show the proportion of replicates found extinct on day 20 in an assay starting from single individuals. Filled circles and error bars represent mean model predictions ± 95% confidence interval. Open symbols represent the observed proportions for the different parasite selection lines (5 lines per selection treatment).

12

SI 4: Epidemiological model fits
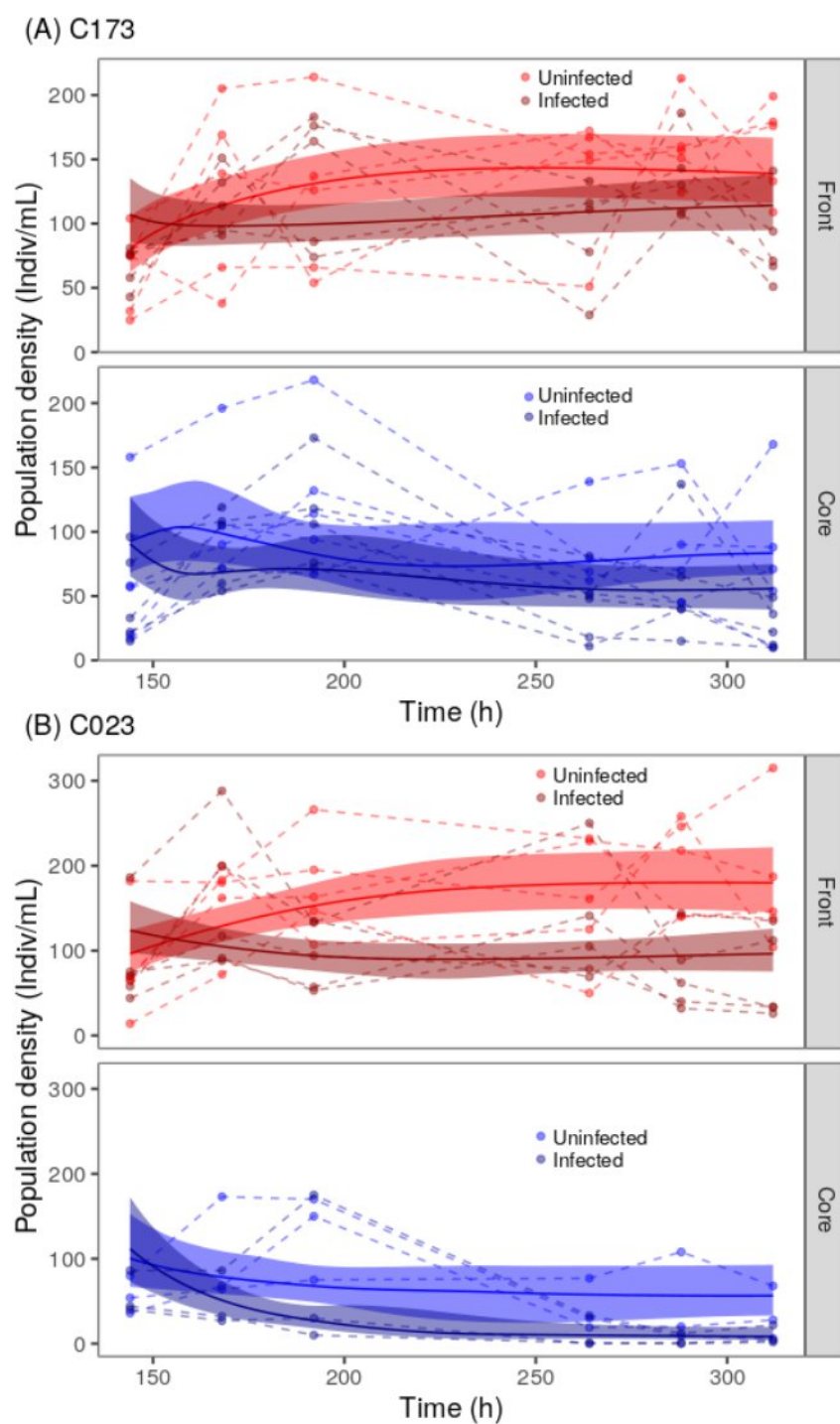
Figure S11. Fit of the epidemiological model (equations 6-8) to infected and uninfected host density time series data in the core and front treatment for host genotype (A) C173 and (B) C023. Dashed lines show observed density trajectories, solid lines and shaded areas represent posterior model predictions.

260